Author Manuscript Published OnlineFirst on June 8, 2021; DOI: 10.1158/2159-8290.CD-20-1378
Author manuscripts have been peer reviewed and accepted for publication but have not yet been edited.

Title: AXL inhibition in macrophages stimulates host-*versus*-leukemia immunity and eradicates naive and treatment resistant leukemia

Irene Tirado-Gonzalez[1,*], Arnaud Descot[1,*], Devona Soetopo[1,*], Aleksandra Nevmerzhitskaya[1], Alexander Schäffer[1], Ivan-Maximilano Kur[1], Ewelina Czlonka[1], Carolin Wachtel[1], Ioanna Tsoukala[1], Luise Müller[2], Anna-Lena Schäfer[1], Maresa Weitmann[1], Petra Dinse[1], Emily Alberto[3], Michèle C. Buck[4], Jonathan JM. Landry[5], Bianka Baying[5], Julia Slotta-Huspenina[6,7], Jenny Roesler[8], Patrick N. Harter[8,9,10], Anne-Sophie Kubasch[11], Jörn Meinel[12], Eiman Elwakeel[13], Elisabeth Strack[13], Christine Tran Quang[14,15], Omar Abdel-Wahab[16], Marc Schmitz[2,10], Andreas Weigert[10,13], Tobias Schmid[13], Uwe Platzbecker[10,11,17], Vladimir Benes[5], Jacques Ghysdael[14,15], Halvard Bonig[18], Katharina S. Götze[4,5], Carla V. Rothlin[3,19], Sourav Ghosh[19,20], Hind Medyouf[1,9,10]

Affiliations:

[1] Institute for Tumor Biology and Experimental Therapy, Georg-Speyer-Haus, Frankfurt am Main, Germany.

[2] Institute of Immunology, Medical Faculty Carl Gustav Carus, TU Dresden, Germany.

[3] Department of Immunology, Yale School of Medicine, New Haven, CT, USA.

[4] Department of Medicine III, Technical University of Munich, Munich, Germany.

[5] Genomics Core Facility, European Molecular Biology Laboratory (EMBL), Heidelberg, Germany.

[6] Department of Pathology, Technical University of Munich, Munich, Germany.

[7] Tissue biobank, Klinikum rechts der Isar and medical faculty Munich (MTBIO), Germany.

[8] Institute of Neurology (Edinger-Institute), University Hospital Frankfurt, Goethe University, Germany.

[9] Frankfurt Cancer Institute, Goethe University, Frankfurt am Main, Germany.

[10] German Cancer consortium (DKTK) & German Cancer Research Center (DKFZ), Heidelberg, Germany.

[11] Medical Clinic and Policlinic 1, Hematology and Cellular Therapy, University Hospital Leipzig, Germany.

[12] Institute of Pathology, University Hospital Carl Gustav Carus, Technical University of Dresden, Germany.

[13] Institute of Biochemistry I, Faculty of Medicine, Goethe-University Frankfurt, 60590 Frankfurt, Germany.

[14] Institut Curie, PSL Research University, CNRS UMR 3348, Orsay, France.

[15] Université Paris Sud, Université Paris-Saclay, Orsay, France.

[16] Department of Medicine, Memorial Sloan Kettering Cancer Center, New York, NY, USA.

[17] Department of Hematology, University Hospital Carl Gustav Carus, Technical University of Dresden, Germany.

[18] Institute of Transfusion Medicine and Immunohematology, Goethe University, and German. Red Cross Blood Service Baden-Württemberg-Hessen, Frankfurt/Main, Germany.

[19] Department of Pharmacology, Yale School of Medicine, New Haven, CT, USA.

[20] Department of Neurology, Yale School of Medicine, New Haven, CT, USA.

* These authors contributed equally

Running title:

AXL blockade elicits anti-leukemic immunity and PD1 blockade

Key words:

Leukemia, Tumor microenvironment, Innate checkpoint, Macrophages, AXL

Financial support:

Research support was provided by the European Research Council to H.M. (ERC-Stg-639795), the EMBO Young Investigator program to H.M. (#4027), the LOEWE Center Frankfurt Cancer Institute (FCI) funded by the Hessen State Ministry for Higher Education, Research and the Arts to H.M., the German Research Council (DFG ME4214/2-1 within SPP 2084) to H.M. and the German Cancer Consortium (DKTK) Joint Funding (CHOICE consortium) to H.M, U.P and K.G. E.C was supported by a fellowship from the German José Carreras Leukemia Foundation (DJCLS 04FN /2018). K.G is supported by the German Research Council (DFG, SFB 1243 project A09) and the German Jose Carreras Leukemia Foundation (DJCLS, 14 R/2018).

Corresponding author:

Hind Medyouf, Ph.D.

Institute for Tumor Biology and Experimental Therapy, Georg-Speyer-Haus, Paul-Ehrlich Strasse, 42-44, 60596, Frankfurt am Main, Germany. e-mail: medyouf@gsh.uni-frankfurt.de
Tel: +49 6963395540

Conflict of interest

H. Medyouf has received research support from Janssen and Bergenbio, ASA and consulted for Bergenbio, ASA within the last 3 years, for projects that are unrelated to this study. No potential conflicts of interest were disclosed by the other authors.

Author Manuscript Published OnlineFirst on June 8, 2021; DOI: 10.1158/2159-8290.CD-20-1378
Author manuscripts have been peer reviewed and accepted for publication but have not yet been edited.

ABSTRACT

Acute leukemias are systemic malignancies associated with a dire outcome. Due to low immunogenicity, leukemias display a remarkable ability to evade immune control and are often resistant to checkpoint blockade. Here, we discover that leukemia cells actively establish a suppressive environment to prevent immune attacks by co-opting a signaling axis that skews macrophages towards a tumor promoting tissue repair phenotype, namely the GAS6/AXL axis. Using aggressive leukemia models, we demonstrate that ablation of the AXL receptor specifically in macrophages, or its ligand GAS6 in the environment, stimulates anti-leukemic immunity and elicits effective and lasting NK- and T-cell dependent immune response against naive and treatment resistant leukemia. Remarkably, AXL deficiency in macrophages also enables PD1 checkpoint blockade in PD1-refractory leukemias. Lastly, we provide proof-of-concept that a clinical grade AXL inhibitor can be used in combination with standard of care therapy to cure established leukemia, regardless on AXL expression in malignant cells.

Author Manuscript Published OnlineFirst on June 8, 2021; DOI: 10.1158/2159-8290.CD-20-1378
Author manuscripts have been peer reviewed and accepted for publication but have not yet been edited.

STATEMENT OF SIGNIFICANCE

Alternatively primed myeloid cells predict negative outcome in leukemia. By demonstrating that leukemia cells actively evade immune control by engaging AXL RTK in macrophages and promoting their alternative priming, we identified a target which blockade, using a clinical grade inhibitor, is vital to unleashing the therapeutic potential of myeloid-centered immunotherapy.

Author Manuscript Published OnlineFirst on June 8, 2021; DOI: 10.1158/2159-8290.CD-20-1378
Author manuscripts have been peer reviewed and accepted for publication but have not yet been edited.

INTRODUCTION

Acute leukemia is a heterogenous group of devastating and rapidly progressing blood cancers that have a dismal outcome. Despite therapeutic progress, acute leukemia remains the leading cause of cancer-related death in children and is an appalling clinical challenge in particular in adults and elderly, whose overall survival (OS) remains below 50% (1,2). Similar to solid cancers, immune evasion is a hallmark of acute leukemia (3). Several studies have identified leukemia intrinsic mechanisms that promote immune escape, including loss of HLA molecules (4-6), expression of inhibitory ligands that dampen T cell response (7) as well as downregulation of ligands that activate cytotoxic lymphocytes, such as NK cells (8). Moreover, the disseminated nature of acute leukemia, their rapid disease course as well as their notoriously low mutational load (9) represent specific features that likely limit the initial engagement of anti-leukemic immunity (3,10). This is exemplified by the recent finding that disseminated acute myeloid leukemia (AML) cells fail to induce host type I interferon response and effective anti-leukemic immunity (11). Besides these leukemia intrinsic features, the extrinsic environment is also believed to heavily contribute to immune evasion, but the underlying molecular mechanisms remain largely unknown in hematological malignancies. Therefore, identifying the pathways that impose a suppressive environment is critical to close this gap in knowledge and inform the development of more effective therapies.

Tumor associated myeloid cells significantly impact tumor progression through a plethora of mechanisms including dampening protective adaptive immunity (12). In B-cell acute lymphoblastic leukemia (B-ALL), a recent single cell RNA study revealed that monocyte abundance, and in particular non-classical monocytes, is predictive of patient's survival (13). Likewise, high number of $CD68^{+}CD163^{+}$ M2-like macrophages or CD206 immune suppressive myeloid cells are associated with poor outcome in adult T-cell leukemia and AML, respectively (14,15). These studies suggest, that similar to their counterpart found in solid tumors, leukemia associated myeloid cells likely contribute to disease progression, however, the underlying molecular mechanisms remain undefined.

Under physiological conditions, a well-known immune regulatory mechanism, that is primarily active in myeloid cells, is driven by the TYRO3, AXL and MERTK (collectively termed TAM) receptor tyrosine kinases (RTKs). These RTKs are differentially activated by their ligands GAS6 and PROS1, with GAS6 showing highest affinity for AXL. When engaged

in innate immune cells, namely macrophages and dendritic cells (DCs), TAM RTKs drive the acquisition of a non-inflammatory phenotype that promotes tissue-repair and resolution of inflammation (16-18). In cancer, AXL overexpression is frequently associated with poor prognosis, both in solid and hematological malignancies (19). This tumor promoting function of AXL is primarily attributed to its tumor cell intrinsic ability to promote proliferation, epithelial to mesenchymal transition, survival and resistance to cancer therapy, including in hematological malignancies (20-29). Additionally, tumor intrinsic AXL expression can exert immune-suppressive functions by suppression of MHC-I expression, induction of PDL1 expression and altered expression of cytokines and chemokines that promote recruitment of myeloid cells (30-36). Notably, although AXL is expressed in immune cells within the tumor microenvironment, its potential tumor immune modulatory function in tumor-associated immune cells *per se*, remains largely unexplored.

Here we demonstrate that acute leukemia cells establish a self-reinforcing immune suppressive microenvironment by co-opting a host-derived mechanism, driven by GAS6/ AXL axis in macrophages, to dampen innate immunity and limit protective inflammation. Combining different mouse models and clinical grade pharmacological inhibitors, we show that targeting AXL specifically in macrophages, promotes anti-leukemic immunity, and elicits susceptibility to PD1 blockade. When further combined with the standard of care treatment, GAS6/AXL blockade leads to unprecedented cure rates in high-risk B-ALL in mice, including those resistant to BCR-ABL1 inhibition.

RESULTS

GAS6 is induced in the bone marrow microenvironment of patients with hematological malignancies and its expression correlates with poor outcome.

Using publicly available data sets, we found that high *GAS6* expression correlates with poor outcome in acute myeloid leukemia (AML), the most frequent form of acute leukemia in adults, as well as B-cell lymphoma (Fig. 1A, Supplementary Fig. S1A). Consistently, high *GAS6* expression was previously associated with high-risk adult patients with *de novo* AML (28). To extend these *in-silico* findings to other hematological malignancies, and pinpoint the cellular source of GAS6, we used immune-histochemistry (IHC) to evaluate GAS6 expression *in situ*, in bone marrow trephine biopsies from B-cell and T-cell acute lymphoblastic leukemia (B-ALL and T-ALL) patients, at diagnosis (Table S1). In B-ALL,

Author Manuscript Published OnlineFirst on June 8, 2021; DOI: 10.1158/2159-8290.CD-20-1378
Author manuscripts have been peer reviewed and accepted for publication but have not yet been edited.

GAS6 was undetectable in malignant blasts marked by CD10 expression (Fig. 1B, top left panel), that often constitute over 95% of the cells in diagnostic biopsies, and readily produced by stromal cells, megakaryocytes and hematopoietic cells with typical myeloid morphology (Fig. 1B, Supplementary Fig. S1B). Using an *ex-vivo* co-culture system, we show that both Philadelphia chromosome positive (Ph+) B-ALL and myeloid leukemia cells (MDS and AML) instructively enhance *GAS6* expression in human monocytes ($CD14^+$) isolated from healthy donors (Fig. 1C). Overall, these human data indicate that leukemic cells enhance *GAS6* expression in the microenvironment in a spectrum of hematological malignancies and most importantly, that *GAS6* expression correlates with poor outcome.

Induction of successful anti-leukemic immunity by *Gas6* ablation in the host environment

To functionally test the role of GAS6 in possibly abetting leukemia progression, three syngeneic leukemia models were used in this study. In the myeloid models, disease was initiated by either the loss of *Asxl1* (37) (Supplementary Fig. S1C-H and Supplementary Methods) or the expression of the MLL-ENL fusion oncogene coupled to a tomato reporter (38) (Supplementary Fig. S1I). For lymphoblastic leukemia, we used a highly aggressive B-ALL model driven by the expression of the BCR-ABL1 fusion oncogene coupled to GFP, in an *Arf* null genetic background (Supplementary Fig. S1J-L). This secondary genetic lesion is frequently found in high-risk B-ALL patients bearing the Philadelphia chromosome (Ph^+, the chromosomal translocation encoding the BCR-ABL1 oncoprotein) and is associated with an inferior outcome (39). Leukemic burden was defined by the percentage of $B220^{dim}GFP^+$ and $CD11b^{dim}$ $tomato^+$ cells in the B-ALL and MLL-ENL models, respectively. The Asxl1 model was characterized by massive hepatosplenomegaly and myeloblast infiltration, hence, spleen and liver weight were often used as a surrogate for disease burden (Supplementary Fig. S1F-G). Notably, all three disease models show undetectable leukemia-intrinsic expression of *Axl* and *Mertk*, but do express *Tyro3*, albeit at variable levels (Supplementary Fig. S2A-J), and therefore could possibly derive cell-intrinsic benefit from Gas6 in the microenvironment, as previously reported by others (20-25,27,28,40). In line with the human data, we show increased Gas6 protein expression in leukemia associated $Iba1^+$ myeloid cells (Supplementary Fig. S2K). Several cytokines are proposed to induce *Gas6* expression, including TSG6, IL4, M-CSF and IL10 (22,41). We found *Il10* to be readily upregulated by B-

ALL blasts upon *in vivo* transplantation (Supplementary Fig. S2L). Moreover, IL10 blockade using a neutralizing antibody *in vivo*, significantly blunts GAS6 induction and dramatically reduces the positive correlation seen between the percentage of GFP^+ leukemic blasts and GAS6-expressing $Iba1^+$ myeloid cells (Supplementary Fig. S2M-O). These data demonstrate that IL10, at least in part, contributes to GAS6 induction in leukemia-associated macrophages.

To functionally distinguish between the possibilities that GAS6 stimulates leukemic growth by activating oncogenic TAM receptor signaling in the blasts *versus* whether GAS6 functions *via* negatively regulating the anti-leukemic immune response, we transplanted established leukemia, from three different models, to wild-type (WT) and newly generated *Gas6*-deficient (*Gas6*$^{-/-}$) hosts in a C57BL/6 immune-competent or a *NOD.Cg-Prkdcscid IL2rgtmWjl/Sz* (NSG) severely immune compromised backgrounds (Fig. 1D-O and Supplementary Fig. S3A-D). In all three models, leukemic burden was significantly reduced in immune competent (Fig. 1E, 1I and 1M) but not immune-compromised (Fig. 1F, 1J, 1N, Supplementary Fig. S3E) *Gas6*-deficient animals. The reduction in leukemic burden observed in immune-competent *Gas6*-deficient animals translated in significantly prolonged survivals, in the myeloid disease models (Fig. 1G, 1K), but not in the aggressive B-ALL model (Fig. 1O). Together, these data demonstrate that the functional relevance of GAS6 in leukemia goes well-beyond its previously recognized role as a cell-intrinsic growth promoting factor and relies on its ability to effectively suppress the immune response against leukemia.

GAS6 deficiency synergizes with standard of care therapy to enable a powerful and durable anti-leukemic immune response against BCR-ABL1 positive B-ALL

In the clinical setting, the standard of care for Ph^+ B-ALL patients combines a tyrosine kinase inhibitor (TKI) targeting the ABL1 kinase and intensive chemotherapy (including vincristine) followed by allogeneic hematopoietic cell transplantation (HCT) for clinically fit adult patients. Because efferocytic clearance of apoptotic cells by TAM receptors expressing phagocytes, promotes the resolution of inflammation both by avoiding secondary inflammatory cell death and altering phagocyte priming (42), we speculated that induction of apoptotic cell death, may synergize with a *Gas6*-deficient environment to promote anti-tumor immunity. Leukemia challenged immune competent *WT* and *Gas6*$^{-/-}$ mice were therefore subjected to a second-generation tyrosine kinase inhibitor targeting the BCR-ABL1 oncogene (nilotinib) and

vincristine treatment (Fig. 1P), both of which induce effective apoptotic cell death. While vehicle treated animals rapidly succumbed to leukemia with a median survival of 20 days, regardless on genotype (Fig. 1Q), 70% (9/13) of nilotinib plus vincristine treated *Gas6*$^{-/-}$ mice remained leukemia free and achieved long-term disease-free survival (Fig. 1Q, Supplementary Fig. S4A). In stark contrast, only 30% (4/12) of WT mice showed durable responses (Fig. 1Q, Supplementary Fig. S4A), a result that is well in line with the 5-year overall survival (OS) observed in patients (43). Additionally, bone marrow cells from long-lived *Gas6*$^{-/-}$ mice failed to transfer disease to secondary immune-compromised NSG hosts (Supplementary Fig. S4B), thereby demonstrating leukemia eradication in the primary hosts.

To further model the clinical situation often encountered with elderly and frail Ph^{+} B-ALL patients that cannot tolerate intensive chemotherapy, we also evaluated the impact of treatment with nilotinib alone. Although nilotinib-treated WT mice showed a significantly prolonged survival, they ultimately succumbed to full blown leukemia (Supplementary Fig. S4C), hence recapitulating the relapses seen in patients treated with TKI alone (44). In stark contrast, 30% (3/10) of nilotinib-treated *Gas6*$^{-/-}$ mice showed durable responses and remained leukemia free (Supplementary Fig. S4C). Bone marrow cells from long lived nilotinib-treated *Gas6*$^{-/-}$ mice also failed to propagate leukemia upon transfer to secondary NSG recipients, indicating effective cure of the primary host (Supplementary Fig. S4D). Importantly, when immune compromised NSG mice, bearing the same leukemia cells, were subjected to the same treatment, the synergistic effects between *Gas6* deficiency and nilotinib were abrogated (Supplementary Fig. S4E). Together, these data unequivocally show that blockade of GAS6-mediated immune suppression effectively synergizes with standard of care regimens to achieve eradication of leukemic stem cells (i.e. cells with leukemia propagating activity) in B-ALL, thereby leading to long-term disease-free survival. This new strategy could considerably enhance the effectiveness of TKI treatment in frail patients that are urgently in need for alternative therapeutic approaches.

AXL-expressing leukemia-associated macrophages contribute to immune suppression.

AXL, the TAM RTK with the highest affinity for GAS6, is readily expressed in leukemia associated myeloid cells, in particular, Iba1^{+} macrophages (Fig. 2A). High *Axl* expression in mononuclear phagocytes, namely monocytes, macrophages and dendritic cells

Author Manuscript Published OnlineFirst on June 8, 2021; DOI: 10.1158/2159-8290.CD-20-1378
Author manuscripts have been peer reviewed and accepted for publication but have not yet been edited.

(45) was also seen using the Immunological Genome project (https://www.immgen.org) (Supplementary Fig. S5A). We next speculated that GAS6 expression could promote leukemic progression by signaling through AXL in immune cells and tested whether selective *Axl* deletion in leukemia associated myeloid cells (both macrophages and DCs) enhances anti-leukemic immunity using mice with floxed alleles of *Axl* plus a Cre recombinase driven by the *Csf1r* promoter (*Csf1r-Cre*$^{+}$ *Axl*$^{f/f}$), as previously described (42) (Supplementary Fig. S5B). When challenged with B-ALL, control mice (*Axl*$^{f/f}$) exhibited full-blown leukemia, while *Csf1r-Cre*$^{+}$ *Axl*$^{f/f}$ mice showed no sign of disease as evidenced by macroscopic analysis, flow cytometry and IHC (Fig. 2B, Supplementary Fig. S5C-E). Remarkably, this translated into long-term DFS of >140 days in 80% of the animals (Fig. 2C). Long-term survivors had no detectable GFP^{+} leukemia cells in the bone marrow, indicating effective leukemia clearance (Supplementary Fig. S5F). Potential *Csf1r-Cre* toxicity was carefully excluded as both *Axl*$^{f/+}$ and *Csf1r-Cre*$^{+}$ *Axl*$^{f/+}$ mice had full-blown leukemia after challenge with B-ALL (Supplementary Fig. S5G-H). Notably, myeloid specific *Axl* deletion has more prominent anti-leukemic effects than constitutive *Gas6* loss in B-ALL (Compare Fig. 1M and 1O to Fig. 2B and 2C). We speculate this might be mitigated by the increased expression of other TAM receptors ligands, such as *Pros1*, which is significantly induced in macrophages in response to B-ALL, but not AML (Supplementary Fig. S5I). Similar to GAS6, PROS1 promotes the resolution of inflammation by phagocytes (16) and tumor derived PROS1 has been proposed to limit anti-tumor immune response in the B16F10 melanoma model (46).

Because of its physiological expression in DCs and the recent finding that AXL partially marks a subpopulation of immunoregulatory DCs that restrain DC immuno-stimulatory function, termed mregDCs (47), we also explored the impact of selective *Axl* deletion in DCs, using the *CD11c-eGFP-Cre* line, as previously reported (Supplementary Fig. S5B)(48). We found that *Axl* deletion in DCs alone, is not sufficient to elicit anti-leukemic immunity (Fig. 2D), while depletion of macrophages, using clodronate liposomes in *Csf1r-Cre*$^{+}$ *Axl*$^{f/f}$ mice prior to leukemia challenge abolished anti-leukemic immunity (Fig. 2E, Supplementary Fig. S5J). Importantly, the anti-leukemic effects and prolongation of survival conferred by *Axl* deletion in *Csf1r*-expressing cells were also recapitulated in the myeloid leukemia models (Fig. 2F-I). Likewise, AML burden remained unaffected when *Axl* was specifically ablated in DCs (Fig. 2J), further confirming the finding from the B-ALL model. Notably however, *Axl*-deficiency did not lead to cure in the MLL-ENL model, possibly

Author Manuscript Published OnlineFirst on June 8, 2021; DOI: 10.1158/2159-8290.CD-20-1378
Author manuscripts have been peer reviewed and accepted for publication but have not yet been edited.

reflecting a difference in the downstream immune response to these different types of leukemia. Collectively, these data point to AXL as a *bona fide* innate immune checkpoint in leukemia-associated macrophages.

AXL ablation in leukemia-associated macrophages prevents the establishment of an immune suppressive microenvironment.

To further characterize the immune changes associated with leukemia and hampered by AXL ablation in macrophages, we FACS purified non-leukemic CD45$^+$ spleen leukocytes from *Axl$^{f/f}$* control and *Csf1r-Cre$^+$Axl$^{f/f}$* animals that were either challenged or not with B-ALL, and subsequently subjected them to scRNAseq using the 10X Genomics platform. A total of 36000 cells, with a median number of 1529 quantified genes/cell were analyzed. Downstream analysis (detailed in the Methods section) identified distinct clusters that were subsequently classified into major hematopoietic cell types (Fig. 3A).To confirm the validity of the inferred cell types, we identified conserved gene markers for each cluster and evaluated their expression across all identified clusters (Fig. 3B, Supplementary Fig. S6A). In response to leukemia, *Axl$^{f/f}$* animals showed a marked expansion of the monocytes and granulocytes clusters with a massive drop in lymphoid cells, likely reflecting the accumulation of immune suppressive myeloid populations (Fig. 3C) including monocytes, which have recently been linked to poor outcome in both adult and childhood BCR-ABL1$^+$ B-ALL (13). These immune suppressive changes, including the accumulation of immune suppressive CD11b$^+$Ly6G$^-$ Ly6C^{high} myeloid derived suppressor cells (MDSCs), were abrogated upon Axl ablation in *Csf1r*-expressing cells (Fig. 3C) and verified to occur both in the spleen and bone marrow, using flow cytometry (Supplementary Fig. S6B and S6C). Differential gene expression (DGE) analysis further revealed that leukemia-challenged *Csf1r-Cre$^+$Axl$^{f/f}$* macrophages display reduced expression of proliferation associated genes (*Pclaf, H2afz, Hspa8*) and drastic decrease in Stathmin expression (*Stmn1*), a microtubule binding protein downregulation of which is required for classical priming of macrophages (49), as well as *Ccl24*, a chemokine that is highly expressed in M2 polarized macrophages (50) (Fig. 3D). Targeted expression analysis of key polarization genes additionally showed that, in response to leukemia challenge, *Axl*-deficient macrophages, exhibit an enhanced expression of immune-stimulatory cytokines (*Il12, Tnfα*)(51,52) and blunted expression of genes associated with tissue-repair and immune-suppressive functions (*Retnla*, *Chil3*, *Il10, Arg1*

Author Manuscript Published OnlineFirst on June 8, 2021; DOI: 10.1158/2159-8290.CD-20-1378
Author manuscripts have been peer reviewed and accepted for publication but have not yet been edited.

and *Tgfb*)*(53)* (Fig. 3E), which further support the single cell transcriptomic results. Of note, detection of these genes in the scRNAseq results was hampered by the limited number of recovered macrophages and DCs, as well as the sequencing depth achieved with the 10X Genomics platform. Besides macrophages, DCs from *Csf1rCre*$^{+}$*Axl*$^{f/f}$ mice also displayed increased expression of the immune stimulatory cytokine *Il12,* while higher expression of *Il10* was prominent in leukemia challenged *Axl*$^{f/f}$ control animals (Fig. 3F) and correlated with increased abundance of CD11b^{+}CD11c^{+} tolerogenic cDC2 in these mice (Fig. 3G) (54). Ultimately, this prominent shift in myeloid priming resulted in reduced frequency of suppressive Foxp3^{+} T regulatory cells (Supplementary Fig. S6D and S6E), higher ratio of CD8 to CD4 T cells (Supplementary Fig. S6F, S6G and S6H) and higher frequency of NK cells (Supplementary Fig. S6I and S6J), reflecting the potent anti-leukemic immune response observed in *Csf1rCre*$^{+}$*Axl*$^{f/f}$ animals.

In a recent study, systemic blockade of MERTK, another TAM receptor family member, was shown to enhance anti-tumor immunity in the MC38 model of colorectal cancer model by engaging the cGAS-STING pathway in phagocytes (55). In our leukemia model, we found STING expression in immune cells to be dispensable for the leukemia rejection phenotype imposed by AXL blockade (Supplementary Fig. S7A-B) while myeloid selective ablation of the suppressor of cytokine signaling 3 (SOCS3) (Supplementary Fig. S7C), an AXL downstream target that actively impairs type I IFN response and pro-inflammatory cytokines signaling, readily recapitulates the protective effects associated with myeloid selective *Axl*-ablation, in all 3 leukemia models (Supplementary Fig. S7D-G). This hints towards a potentially essential role of pro-inflammatory and immune stimulatory cytokines in this process and argues that, although the outcomes of blocking MERTK in the MC38 model, or AXL in leukemia, are similar, the underlying downstream molecular mechanisms are likely distinct.

Axl ablation in leukemia-associated macrophages unleashes an effective NK- and T cells mediated-killing of leukemia cells.

Because the activity of NK cells is tightly modulated by macrophages and greatly enhanced by IL12, we speculated that NKs might be involved in the leukemia clearance phenotype. Intra-peritoneal administration of an anti-NK1.1 antibody every 5 days, starting 2 days before leukemia transplantation, achieved effective and continuous depletion of NK

Author Manuscript Published OnlineFirst on June 8, 2021; DOI: 10.1158/2159-8290.CD-20-1378
Author manuscripts have been peer reviewed and accepted for publication but have not yet been edited.

cells (Supplementary Fig. S7H-I). In B-ALL (Fig. 4A-C) and AML (Fig. 4D-F) challenged mice, both NK depleted, and non-depleted *Axl*$^{f/f}$ control animals showed comparable leukemic burden and succumbed to disease with similar latencies, suggesting that NK cells are functionally impaired. In *Csf1r-Cre*$^{+}$ *Axl*$^{f/f}$ mice however, NK-depletion abrogated anti-leukemic immunity and resulted in an accelerated disease course in both leukemia types, while IgG-treated counterpart remained largely protected against B-ALL (Fig. 4C) and maintained a prolonged survival in AML (Fig. 4F). This demonstrates that *Axl* ablation in phagocytes is sufficient to elicit a powerful NK cell response that is essential for leukemic clearance.

To further interrogate the functional relevance of T cells as additional downstream effectors, we generated compound mice that lack CD8 T cells as well as *Axl* expression in phagocytes (*Csf1r-Cre*$^{+}$ *Axl*$^{f/f}$ *Cd8a*$^{-/-}$ and *Axl*$^{f/f}$ *Cd8a*$^{-/-}$) and challenged them with B-ALL or AML. In B-ALL, CD8 deficiency abrogated the survival advantage observed in *Csf1r-Cre*$^{+}$ *Axl*$^{f/f}$ compared to *Axl*$^{f/f}$ control mice (Fig. 4G, 4H). These results were recapitulated by depletion of CD8^{+} T cells using an antibody approach (Supplementary Fig. S7J-K). Notably, the lower leukemic burden observed in *Csf1r-Cre*$^{+}$ *Axl*$^{f/f}$ *Cd8a*$^{-/-}$ animals may reflect the productive engagement of NK cells that are unaffected in this model. In the MLL-ENL AML model, the survival benefit conferred by *Axl*-deficient phagocytes was maintained in CD8 deficient animals (Fig. 4I, 4J). Together, these data reveal that productive engagement of NK cells is a shared downstream mechanism by which Axl-deficient macrophages elicit anti-leukemic immunity, while the engagement of CD8 T cells appear to be model dependent.

Axl ablation in macrophages elicits susceptibility to PD1-checkpoint blockade in PD-1 refractory treatment naive B-ALL

The fact that the enhanced anti-leukemic immunity observed in B-ALL challenged *Csf1r-Cre*$^{+}$ *Axl*$^{f/f}$ mice depends, at least in part, on T cells, prompted us to test whether interfering with this axis could also sensitize PD-1 refractory B-ALL (Fig. 5A), to PD1 checkpoint blockade therapy. To address this issue, we took advantage of the limited fraction (10-20%) of *Csf1r-Cre*$^{+}$ *Axl*$^{f/f}$ mice that eventually escape immune control and develop leukemia in the B-ALL model with a significantly delayed latency of > 40 days (Fig. 2C). In situ IHC analysis of bone marrow and spleen sections revealed prominent PD1-expression in these mice (Fig. 5B), which was largely restricted to the CD8^{+} T cell subset, as demonstrated

by flow cytometry (Fig. 5C-D). On the other hand, PD1 ligand (PD-L1) is readily expressed by stromal and immune cells in the bone marrow as well as leukemic cells themselves (Fig. 5E). PD1 blockade in *Csf1r-Cre*$^{+}$ *Axl*$^{f/f}$ mice in early stage relapse (up to 2% leukemic burden in PB) led to rapid leukemic clearance (Fig. 5F-G) and long-term DFS of over 120 days (Fig. 5H). Hence our data demonstrate that AXL blockade in phagocytes, not only triggers a potent and lasting immune response against BCR-ABL1^{+} B-ALL, but also elicits susceptibility to checkpoint blockade in case of disease recurrence

AXL inhibition in non-malignant cellular components of the leukemic microenvironment, unleashes a potent anti-leukemic immunity *in vivo* and synergizes with standard of care therapy to eradicate leukemia.

To determine the translational relevance of these findings, we pharmacologically interfered with AXL *in vivo*, using Bemcentinib (also known as R428 or BGB324) (56), an orally available and selective inhibitor for AXL currently undergoing clinical evaluation in cancers in which AXL expression, in tumor cells, is thought to contribute to disease pathogenesis (e.g. NCT02488408; NCT02424617; NCT02922777). In this study, by using leukemia models that do not express AXL protein (Fig. S2J), we primarily used Bemcentinib to evaluate its potential immune modulatory effects on the non-malignant components of the leukemic microenvironment that express AXL, namely myeloid cells (Fig. 2A). To model an intervention trial in which patients would exhibit low leukemic burden, such as those with measurable minimal residual disease (MRD^{+}) after induction therapy, Bemcentinib treatment was initiated several days post-leukemia challenge when leukemic cells were readily detected in the bone marrow and administered 7 days a week, twice daily at a dose of 50 mg/kg body weight. This resulted in reduced AXL phosphorylation in Iba1 expressing macrophages (Fig. 6A) and led to a significant reduction in leukemic burden across all analyzed organs in the highly aggressive B-ALL model (Fig. 6B). As anticipated, in this model, the anti-leukemic effects were dependent on the engagement of CD8 T cells, as demonstrated by the lack of therapeutic efficacy of Bemcentinib in CD8 deficient mice (Fig. 6C). In line with our observations in *Axl* deleted macrophages, Bemcentinib significantly and consistently enhanced the proinflammatory priming of macrophages as evidenced by increased expression of *Il12* and *Tnfα* in response to LPS and IFNγ, *ex vivo* (Supplementary Fig. S8A). Consequently, we show that the therapeutic effects of Bemcentinib are curtailed upon IL12 and TNFα blockade *in vivo* (Fig. 6D), indicating that these pro-inflammatory

cytokines indeed contribute to the overall immune stimulatory effects observed upon AXL inhibition *in vivo*.

To further evaluate whether AXL inhibition may improve overall survival, leukemia bearing mice were first treated with Bemcentinib, as a single agent, on an intermittent schedule of 5 days on, 2 days off for the indicated duration. Under these conditions, Bemcentinib led to a significant increase in overall survival (OS) in the *Asxl1*$^{-/-}$ model (Fig. 7A). These effects were lost in immune-compromised NSG mice, in line with Bemcentinib's predicted effects on AXL positive immune cells (Fig. 7B). Of note, terminally ill mice exhibited the same disease phenotype regardless on treatment status (Supplementary Fig. S8B). In the high-risk B-ALL model, single agent treatment with Bemcentinib (Supplementary Fig. S8C) or nilotinib, (Supplementary Fig. S8D), significantly extended survival but all animals eventually succumbed to *bona fide* B-ALL within 50 days, despite continuous drug treatment. Remarkably, however, combination treatment with nilotinib and Bemcentinib exhibited a prominent synergistic effect that led to complete remission and disease eradication in over 90% (30/33) of the animals, with no sign of drug toxicity (Fig. 7C). Notably, although combination treatment was stopped on day 48, all mice remained leukemia-free, as demonstrated by the analysis of their bone marrow using flow cytometry (Fig. 7D) while vehicle-treated mice succumbed to *bona fide* leukemia within 15-20 days. In this experiment, weekly monitoring revealed that 3 out of 33 mice (9%) treated with nilotinib plus Bemcentinib showed sign of disease recurrence around day 30, at which point these mice were subjected to anti-PD1 treatment. Similar to our observation in relapsing *Csf1r-Cre*$^{+}$ *Axl*$^{f/f}$ mice (Fig. 5), checkpoint blockade led to disease clearance in 2 out of the 3 relapsing mice (Fig. 7E). Additionally, when NSG mice, bearing the same leukemia were subjected to combined treatment with nilotinib and Bemcentinib, the latter failed to drastically potentiate nilotinib effects as demonstrated by the fact that 100% of the mice succumbed to leukemia with a median survival that was comparable to nilotinib only treated animals (Fig. 7F).

AXL inhibition synergizes with chemotherapy to eradicate leukemia and promote disease-free survival in TKI resistant BCR-ABL1^{+} B-ALL.

Because treatment resistance is a major source of relapse and a leading cause of acute-leukemia related deaths, we explored the therapeutic efficacy of AXL inhibition in the context of B-ALL resistant to BCR-ABL1 inhibition. B-ALL cells were exposed to increasing

doses of nilotinib *ex-vivo* to obtain a nilotinib resistant subclone (referred to as TKI^R), that was proven to be equally resistant to nilotinib treatment *in vivo* as shown by the lack of survival advantage (Fig. 7G). This is in stark contrast to the increased survival of nilotinib treated animals challenged with the parental (nilotinib sensitive) B-ALL cells (Supplementary Fig. S8D). Bemcentinib alone did not significantly prolong survival in this TKI^R B-ALL model, while chemotherapy using vincristine showed some efficacy, with 4 out of 12 mice (33.3%) achieving long-term DFS (Fig. 7G). Most importantly, addition of the AXL inhibitor to vincristine showed remarkable synergistic effects, with 22 out of 23 mice (95.6 %) achieving leukemic clearance and long-term DFS of over 180 days (Fig. 7G-H). Additionally, secondary transplantation of bone marrow cells from these long-term survivors failed to propagate disease to secondary NSG recipients, thereby indicating effective eradication of leukemia in the treated mice (Supplementary Fig. S8E-F). Notably, TKI^R blasts remained AXL negative thereby excluding a potential leukemia intrinsic effect of AXL inhibition in this setting (Supplementary Fig. S8G). Together, these data unambiguously demonstrate that systemic AXL inhibition using a clinical grade inhibitor, shows significant immune dependent therapeutic efficacy, that further synergizes with standard of care treatment to promote leukemic clearance, prolong OS and even lead to cure in leukemia-bearing mice, including in a TKI^R setting. Additionally, our findings confirm that similar to *Axl* ablation, pharmacological inhibition of AXL also elicits susceptibility to PD1 checkpoint blockade in case of disease recurrence. Collectively this highlights the broad clinical applicability of this new immunotherapeutic modality which could constitute a life-saving alternative strategy for patients that develop therapy resistant disease.

DISCUSSION

In this study, we show that leukemic cells engage a pathway that physiologically enables the non-inflammatory clearance of apoptotic cells by phagocytes (18), namely the GAS6/AXL axis, to usurp macrophages to evade immune control and convert the environment into a highly immune-suppressive milieu that reinforces leukemic expansion. Additionally, we comprehensively demonstrate that ablating AXL, specifically in leukemia-associated macrophages, or its high affinity ligand GAS6 in the host environment, prevents the establishment of a suppressive immune architecture and converts leukemia cells with notoriously low mutational load (9) into potent immune-stimulatory triggers. This is further

supported by the fact that combining GAS6/AXL blockade with treatment regimens that increase apoptosis of leukemia cells (e.g. TKI, chemotherapy) leads to enhanced anti-leukemic effects. Of utmost clinical importance is the demonstration that these unprecedented anti-leukemic effects can be effectively recapitulated, *in vivo,* by subjecting mice bearing AXL negative leukemias to a selective clinical grade AXL inhibitor (56) that can remarkably synergize with standard of care therapy, such as chemotherapy to potentiate anti-leukemic immunity. In highly aggressive Ph^+ B-ALL, this approach effectively eradicates leukemia propagating stem cells, including in TKI resistant models, an outcome that is unprecedented with current therapies. Additionally, we carefully demonstrate that with both the genetic and pharmacological approach, the observed therapeutic effects are strictly immune dependent, as efficacy can be shown in leukemia-bearing immune competent but not immune deficient animals.

Interestingly, a recent study showed that higher expression of *GAS6* correlates with adverse effects in AML patients who underwent HCT (57). The fact that HCT, the curative potential of which primarily relies on the induction of potent graft-versus-leukemia (GvL) effect, cannot overcome the harmful effects imposed by high *GAS6* expression, further supports our conclusion that *in vivo*, GAS6/AXL axis primarily promotes leukemic progression by its suppressive effects in leukemia-associated immune cells. These finding are of high clinical significance as failure to achieve long-term survival in patients, is primarily due to a high rate of relapse and ability of treatment resistant leukemic stem cells to escape immune control (3). Consequently, AXL inhibition may represent a promising post-remission strategy after HCT to boost the donor immune system to eradicate residual malignant cells and thus prevent relapse. Moreover, because AXL inhibition has remarkable immune-sensitizing effects when combined with reduced intensity single agent chemotherapy regimen (Fig. 7G), a combination treatment could empower the patient's own immune system and provide hope for cure to adult and frail patients that cannot be exposed to intensive chemotherapy or HCT, including those with measurable minimal residual disease (MRD^+) after induction therapy.

Mechanistically, we found that AXL blockade in leukemia associated macrophages triggers productive inflammation, by skewing their priming towards a leukemia suppressive phenotype. This prevents the accumulation of MDSCs and stimulates the acquisition of immune stimulatory features in DCs and production of key cytokines such as IL12 and TNFα,

that we demonstrate to be essential for the potent anti-leukemic immunity observed upon AXL inhibition. In line with our finding, myeloid cells engineered to express high levels of IL12 have recently been shown to reverse immune suppression and activate anti-tumor immunity in pre-clinical models of metastasis (58). Additionally, we show that rewiring of the myeloid compartment in our setting, kick starts the immunity cycle (59) and results in major changes in downstream effector cells, including productive engagement of NK cells, suppression of T regulatory cells, as well as potent CD8 response, the latter being most prominently seen in Ph^+ B-ALL. Notably, in Ph^+ B-ALL, our approach leads to complete eradication of leukemia propagating stem cells and elicits susceptibility to PD1 checkpoint blockade upon relapse, an outcome that is unprecedented in this highly aggressive disease model. We speculate that the differential engagement of CD8 T cells, observed in B-ALL *versus* MLL-ENL AML, may reflect the contribution of leukemia intrinsic determinants, such as the immunogenic potential of specific genetic alterations.

To the best of our knowledge, this study is the first to demonstrate that AXL blockade in leukemia associated myeloid cells, triggers effective and durable anti-leukemic immunity, in particular in highly aggressive acute leukemia subtypes, such as Ph^+ B-ALL. Because tumor associated macrophages (TAMs) are key components of the tumor microenvironment and potent drivers of immune suppression, our study goes well beyond the existing cancer literature that only provides rationale for AXL targeting in AXL positive tumors and warrants the clinical evaluation of AXL targeting strategies in other cancer types, including those with AXL negative tumor cells. Furthermore, while tumors evolve under selective pressure of therapies and rapidly acquire resistance, which may limit the long-term benefits associated with tumor intrinsic AXL inhibition, its targeting in non-malignant tumor-associated immune cells may result in lasting efficacy.

Because of its selectivity towards AXL, Bemcentinib triggers robust anti-leukemic immunity without inducing the autoimmune manifestations that are reported in mice with deletion of all three TAM receptors (60). Bemcentinib has so far showed favorable safety data in three phase II clinical trials in AML (NCT02488408; NCT02424617; NCT02922777) with interim reports providing evidence of TCR repertoire diversification in some patients (61), thereby hinting towards a potential immune modulatory effect. In light of our work, it would be important to extend such studies to other hematological malignancies such as Ph^+ B-ALL, and more specifically evaluate the potential tumor extrinsic immune modulatory

Author Manuscript Published OnlineFirst on June 8, 2021; DOI: 10.1158/2159-8290.CD-20-1378
Author manuscripts have been peer reviewed and accepted for publication but have not yet been edited.

function of AXL targeting compounds, including Bemcentinib and other compounds such as Gilteritinib, a dual FLT3/AXL inhibitor that has shown efficacy in FLT3 mutated relapsed or refractory AML (62)

By demonstrating the key immune suppressive function of the GAS6/AXL axis in leukemia-associated macrophages, this work provides a conceptual advance in our understanding of the molecular mechanisms underlying immune suppression in leukemia and can effectively be translated into a treatment strategy that not only empowers the patient's own immune system to fight leukemia but also be harnessed, in specific contexts, to overcome the major issue of primary resistance to PD1 checkpoint blockade. Collectively, we believe our work paves the way for the design of new combinatorial therapeutic strategies that can enhance the effectiveness of standard and immune-based therapies, while limiting treatment-associated toxicity, in aggregate to significantly improve the outcome of leukemia patients. Moreover, because AXL blockade demonstrates efficacy in AXL negative tumors, this work has far-reaching clinical implications, as it extends the potential clinical benefit of AXL inhibition to a wider population of cancer patients. Within the hematological malignancy field, our study also stands as an important report demonstrating that effective rewiring of alternatively primed macrophages towards a pro-inflammatory fate is sufficient to "lift the barriers" towards potent anti-tumor immunity, kick start the immunity cycle and even elicit susceptibility to PD1 checkpoint blockade in highly aggressive PD1-refractory leukemia. As such, our work puts AXL on the list of promising cancer therapeutic targets that could improve efficacy of current therapeutic strategies by virtue of stimulating the innate immune system.

ACKNOWLEDGEMENTS

We thank Diana Passaro and Owen Williams for the MLL-ENL tomato^{+} leukemia cells, Jan Rehwinkel for the *Sting* deficient bone marrow cells, Lisa Sevenich for the *Socs3* floxed mice, Sophia Thevissen for assistance with animal monitoring and processing, Birgitta E. Michels for help with the analysis of the Immunological Genome Project data, Boris Brill and Margit Wagenblast for assistance with animal applications, Stefan Stein, Annette Trzmiel and Malte Paulsen for assistance with cell sorting, Nathalie Groen for assistance with scRNA sequencing data analysis. We are thankful to Florent Ginhoux and Florian R Greten for helpful discussions and feedback and to BergenBio for providing Bemcentinib for this study. The Klinikum rechts der Isar/Technical University Munich (MTBIO) and the Klinikum Carl Gustav Carus MK1 /Technical University Dresden biobanks are acknowledged for support with collection of human bone marrow biopsies.

AUTHOR CONTRIBUTIONS

H.M. conceived and supervised the study. I.T.G, A.D., D.S., A.N., A.S., I.T., A.L.S., C.T.Q, and H.M., performed the experiments. P.D., J.R., P.H., L.M., M.S. and M.C. B. assisted with IHC and evaluation of human and mouse biopsies or smears; E.C., C.W., M.W., I.K., E.A., E.E., and E.S., provided technical support; J.S.H., A.K., A.M., J.M., H.B., U.P. and K.S.G. provided clinical samples and expertise. J.J.L., B.B., and V.B., provided support for single cell RNA sequencing. J.G. provided the murine BCR-ABL1^{+} B-ALL model and discussed experiments and results. O. A-W. provided the *MxCre Asxl1*$^{f/f}$ mice. S.G. and C.V.R. provided the *CD11c-eGFP-Cre Axl*$^{f/f}$ and *Csf1r-Cre Axl*$^{f/f}$ mice and discussed results. H.M. wrote the manuscript. All authors commented on the manuscript.

LEAD CONTACT AND MATERIALS AVAILABILITY

Further information and requests for resources and reagents may be directed to and will be fulfilled by the Lead Contact, Hind Medyouf (Medyouf@gsh.uni-frankfurt.de). All unique/stable reagents generated in this study are available from the Lead Contact with a completed Materials Transfer Agreement.

METHODS

Animal Studies

MxCre Asxl1$^{f/f}$ mice were a kind gift from Dr. Omar Abdel-Wahab (37) and used to generate a transplantable *Asxl1*$^{-/-}$ AML model after inducible ablation of *Asxl1* in aged animals. All experiments were carried out using cells from a diseased primary mouse that displayed expansion of immature CD11b^{dim}B220^{dim} blasts that transferred leukemia to non-irradiated secondary recipients. Details about the generation of both BCR-ABL1^{+} B-ALL and the serially transplantable *Asxl1*$^{-/-}$ AML models are described in Supplementary Methods and Supplementary Fig. S1. Immune competent C57BL/6N Gas6 knock out mice (Gas6$^{tm1.1(KOMP)Vlcg}$) were obtained from the Knock Out Mouse Project (KOMP) Repository. A scheme (Supplementary Fig. S3A) and detailed description of the knock out allele are available at http://www.mousephenotype.org/data/alleles/MGI:95660/tm1.1(KOMP)Vlcg. Absence of Gas6 was validated by real-time PCR and ELISA (Supplementary Fig. S3B and S3D). For *Gas6*$^{-/-}$ mice, C57BL/6N mice were used as controls (Jackson laboratories; line #005304). In all other experiments with immune competent mice, control wild-type mice were from the C57BL/6J sub-strain (Jackson laboratories; line #000664). For bone marrow transplantation experiments, B6.SJL-*Ptprc*^{a} *Pepc*^{b}*/BoyJ* (CD45.1) were used as recipients (Jax line # 002014). Immune-deficient Gas6 knock out mice were generated by inactivation of the *Gas6* gene using CRISPR-Cas9 editing in *NOD.Cg-Prkdc*^{scid} *IL2rgtmWjl/Sz (NSG)* zygotes using a workflow that was recently described by our group and detailed in Supplementary Methods and Supplementary Fig. S3C (63). NSG mice were obtained from the Jackson Laboratories (Jackson laboratories; line #005557). The *Csf1r-Cre Axl*$^{f/f}$ and *CD11c-eGFP-Cre Axl*$^{f/f}$ mice were obtained from Carla Rothlin and Sourav Ghosh (Yale university, New Haven, CT, USA) and described previously (42,48). *Cd8a*$^{-/-}$ mice (Jax line #002665), *Sting*$^{-/-}$ mice (Jax line # 025805) and *Socs3*$^{f/f}$ mice (Jax line # 010944) were obtained from the Jackson Laboratories. Mice were bred and maintained at the animal facility

of the Institute for Tumor Biology and Experimental Therapy, Frankfurt am Main, Germany in accordance with regulatory guidelines. All experiments were approved under protocols number G50/15, F123/1034 and F123/2003.

Data Reporting

No statistical methods were used to predefine sample size. In drug treatment experiments, mice were randomized to different treatment groups. Mice monitoring was done with blinding.

Cell Lines

The MS-5 cell line was acquired from the DSMZ-German Collection of Microorganisms and Cell Cultures. The PlatE cell line (64) was a gift from Dr. Jacques Ghysdael, and used to generate retroviral stocks expressing BCR-ABL1 as described previously (65). Primary leukemia lines and cell lines were routinely checked for mycoplasma using the Venor GeM OneStep Mycoplasma PCR kit (Minerva Biolabs).

Leukemia Transplantation Experiments

For primary BCR-ABL1^{+} B-ALL generation (Supplementary Fig. S1J), transduced cells were transplanted in lethally irradiated C57BL/6J mice (9 Gy). For all experiments, leukemia cells from primary mice were transplanted in non-irradiated secondary recipients, to maintain the integrity of the microenvironment. The number of cells injected is indicated in each Fig. legend. Generation of BCR-ABL1^{+} B-ALL and a serially transplantable *Asxl1*$^{-/-}$ AML model are described in more details in Supplementary Methods and Supplementary Fig. S1. The MLL-ENL leukemia model has been described previously (38,66). For this model, transplantation of 10^5 leukemic cells (tomato^{+}) cells was used to carry out all described experiments.

Generation of Bone Marrow Chimeras

WT B6.SJL-*Ptprc*^{a} *Pepc*^{b}*/BoyJ* (CD45.1) (Jax line # 002014) mice were lethally irradiated (9 Gy) and subsequently reconstituted by intravenous injection of 1.5 10^6 whole bone marrow cells isolated from either WT C57BL/6J (CD45.2) mice or *Sting* $^{-/-}$ (CD45.2) mice. Hematopoietic reconstitution was verified by bleeding and flow analysis before mice were used in experiments (Supplementary Fig. S7A).

Peripheral Blood Analysis

Blood was collected by bleeding from the *vena facialis* using an EDTA containing microvette (Microvette® 200 K3E, SARSTEDT).

Isolation of human monocytes and co-culture experiments.

Peripheral blood was obtained from healthy adults, and mononuclear cells isolated by Ficoll density gradient centrifugation using Ficoll-Paque Plus (1077 g/ml; GE Healthcare). Monocytes were isolated using MACS Human CD14 microbeads (#130-050-201; Miltenyi Biotec) according to the manufacturer's instructions. Purity was confirmed by FACS to be > 95%. Co-cultures of monocytes and Cell Trace Violet (Invitrogen, #C34557) labelled leukemia cells were carried out in StemSpan serum free medium (Stem Cell Technologies) supplemented with 1% penicillin/streptomycin and glutamine for 24h in 12-well plates. $CD45^{+}CD14^{+}$ monocytes were subsequently purified using flow-cytometry before RNA was isolated using the PicoPure™ RNA Isolation Kit (Applied Biosystems, #KIT0204).

RNA Isolation and Real-time PCR

Spleen-derived macrophages were obtained using ultrapure mouse anti-F4/80 microbeads (#130-110-443, Miltenyi Biotec) as per-manufacturer's instructions. Purified cells were verified to be least 95% $CD45^{+}CD11b^{+}F4/80^{+}$. Assessment of *Axl* excision in the *Csf1r-Cre*$^{+}$ *Axl*$^{f/f}$ mice has been evaluated as previously described (42)**.** RNA was isolated using the PicoPure™ RNA Isolation Kit (Applied Biosystems, #KIT0204) according to the manufacturer's instructions and converted into cDNA using the SuperScript® VILO™ cDNA Synthesis Kit (Thermo Fischer Scientific, #11754050). cDNA was diluted 1:4 before usage. Real-time PCR for assessment of *Axl* excision was carried out using *Axl* primers described in (42) and expression was normalized to *Sdha.* Primers were purchased from Sigma-Aldrich and sequences provided in Supplementary Methods. ABI Power SYBR Green Master Mix (#4368702, Thermo Fischer Scientific) was used. For all other real-time PCR experiments, taqman based real-time PCR assays using the TaqMan™ Gene Expression Master Mix (Thermo Fisher Scientific, #4369016) and taqman probes listed in Supplementary Methods, all purchased from Thermo Fisher Scientific. Reactions were all performed on Viia7 system (Thermo Fisher Scientific).

Author Manuscript Published OnlineFirst on June 8, 2021; DOI: 10.1158/2159-8290.CD-20-1378
Author manuscripts have been peer reviewed and accepted for publication but have not yet been edited.

Analysis of Publicly Available Datasets

RSEM-normalized RNA-seq expression data of 173 primary AML samples from The Cancer Genome Atlas (TCGA-LAML)(67) and corresponding clinical data were downloaded using the cBioPortal for Cancer Genomics (https://www.cbioportal.org). The B-cell lymphoma dataset (GSE4475, n=159) was retrieved from The SurvExpress database (68). Both datasets were imported into the R2 Genomics Analysis and Visualization Platform (http://r2.amc.nl) and subjected to a KaplanScan analysis to stratify patients according to *GAS6* expression using the "scan" mode to define the best expression cutoff. Results were exported and plotted using GraphPad Prism 7 software and survival analysis performed using the log-rank (Mantel–Cox) test.

Flow Cytometry

Cells were prepared as single cell suspension and blocked with CD16/32 Fc Block (BD Biosciences, #553441) then subjected to multicolor panel staining. Staining was performed for 45 mn on ice, in the dark. Antibodies and secondary reagents were titrated to determine optimal concentrations. CompBeads (BD Biosciences) were used for single-color compensation to create multi-color compensation matrices. The mouse antibodies used in this study were as follows: anti-CD45 BV786 (BD Biosciences, #564225), anti-CD45.1 FITC (eBioscience, #11-0453-85), anti-CD45.2 PE (eBioscience, #12-0454-83), anti-Gr1 PE-Cy7 (BD Biosciences, #552985) , anti-CD3 APC-CY7 (Biolegend, #100222), anti-CD8a AF700 (BD Biosciences, #564986) or anti-CD8 PECY7 (eBioscience, #25-0081-82), anti-CD4 PECY7 (eBioscience, #25-0041-82), anti-B220 APC (BD Biosciences, #553092) or anti-B220 BV711 (BD Biosciences, #563892), anti-NK1.1 PECF594 (BD Biosciences, #562864), anti-CD11b FITC (BD Biosciences, #553310) or anti-CD11b PECF594 (BD Biosciences, #562317), anti-CD11c AF700 (BD Biosciences, #560583), anti-F4/80 PE (BD Biosciences, #565410), anti-MHC-II BV650 (BD Biosciences, # 563415), anti-Annexin V-APC (BD Biosciences, #550475) and anti-FoxP3 PE (eBioscience, #12-5773-82), anti-Axl APC (eBioscience, #17-1084-82), anti-DX5 APC (eBioscience, #17-5971-81). The human antibodies used in this study were as follows: hCD45 PE (BD Bioscience; cat 555483), hCD14 APC-CY7 (BD bioscience; Cat 557831). For Foxp3 staining, following cell surface staining cells were fixed and permeabilized using the Cytofix/Cytoperm plus (BD

Biosciences, #555028) according to the manufacturer instructions and Foxp3 staining was performed overnight, at 4C in dark using an antibody dilution of 1:200. Propidium iodide (Cas No. 25535-16-4, Sigma-Aldrich) or the AF700 fixable viability dye (BD bioscience; cat 564997) was used for live- and dead-cell discrimination. Gating strategies are depicted in main and Supplementary Figures. FACS data were acquired on a BD LSRFortessa™ (BD Biosciences). Fluorescence-activated cell sorting (FACS) was done using a FACSAria™ Fusion (BD Biosciences, Heidelberg, Germany). BD FACS Diva software version 8.0.1 was used for data collection. FlowJo version 10.4.2 was used for data analysis. Post-sort purity was >95% and determined by re-analysis of sorted Cells.

Single cell RNA sequencing

Viable non-leukemic (GFP^-) leukocytes were FACS sorted from the spleen of n = 8 mice (No leukemia *Axl*$^{f/f}$, n = 2; no leukemia *Csf1r-Cre*$^+$ *Axl*$^{f/f}$, n = 2; B-ALL *Axl*$^{f/f}$, n = 2; B-*ALL Csf1r-Cre*$^+$ *Axl*$^{f/f}$, n = 2) and subjected to single cell RNA sequencing following a standard 10X Genomics workflow. Libraries were generated using the Chromium Next GEM Single Cell 3' v3.1 kit. cDNA QC and quantification was measured using Bioanalyzer High Sensitivity DNA chip (Agilent) and Qubit dsDNA High Sensitivity kit (Thermo Fisher Scientific). The sequencing was performed on NextSeq500 platform (Illumina) with a sequencing depth of at least 20,000 reads per cell using the NextSeq500/550 high output kit v2.5 (75 cycles) (Illumina; cat 20024906). 2 runs were conducted, thus generating 2 libraries, using 1 mouse from each condition. 10X Genomics demultiplexed sequencing reads were obtained using cellranger mkfastq (version 3.1.0) from 10X Genomics and used to align the reads to the mouse genome (refdata-cellranger-mm10-3.0.0). The data from all samples were loaded in R (R version 3.6.2) and processed using the Seurat package (version 3.2.0) (69). Cells with at least 1000 UMI's per cell and less than 20% mitochondrial gene content were retained for analysis. To increase our analytical power, data from all mice, regardless on genotype or disease status, were initially combined into a single set leading to a total cell number of 36000 cells. Merged dataset was normalized for sequencing depth per cell and log-transformed using a scaling factor of 10,000. The most variable genes in the dataset were identified and the top 2000 was used for dimensionality reduction using Uniform Manifold Approximation and Projection (UMAP) dimension reduction technique (70) followed by density-based clustering using the Seurat tool (69). The top differentially expressed genes

per cluster were used to identify cell types. To evaluate the differences between samples, differential expression analysis was performed using the MAST test using the 10X run number as latent variable (71).

Administration of Drugs

Nilotinib (cas Nr- 641571-10-0) was purchased from APExBIO (APExBio, Houston, USA) and administered once daily by oral gavage at a dose of 80 mg/kg (72). Bemcentininb (BGB324; cas Nr-1037624-75-1) was kindly provided by BergenBio, ASA and administered twice daily by oral gavage at a dose of 50 mg/kg as previously reported (35). Vincristine sulfate was purchased from APExBIO (Cas Nr-2068-78-2) and administered by intra-peritoneal injection (i.p.) once a week at a dose of 0.5 mg/kg for 2 weeks. The vehicle used for both Bemcentinib and nilotinib was 0.5 % (W/W) Methyl Cellulose 400cp (#M0262, Sigma-Aldrich) / 0.1 % (W/W) Tween 80 (#P4780, Sigma-Aldrich) in water. Vincristine sulfate was prepared in phosphate-buffered saline (PBS). Nilotinib and Bemcentinib were administered on 5 days ON / 2 days OFF schedule, unless otherwise indicated in text or Fig. legends. Nilotinib and Bemcentinib were prepared freshly every day.

ELISA

Peripheral blood serum was isolated using Microvette® 500 Z-Gel (#20.1344**,** SARSTEDT). Samples were then analyzed using the Mouse Gas6 DuoSet ELISA (DY986: R&D Systems), according to the manufacturer's instructions. Results were plotted using GraphPad Prism 7 software.

Generation of Bone Marrow Derived Macrophages and Polarization Experiments

Bone marrow cells from 2 femurs were cultured for 6 days in 30ml size teflon bags (#PL30, PermaLife, Origen) in DMEM (#21969-035, Gibco, Life Technologies) complemented with 10% fetal bovine serum (#10270106, Gibco, Thermo Fischer Scientific), 1% L-Glutamine (#25030-024, Gibco, Thermo Fischer Scientific), 1% HEPES 1M (#H0887, Sigma-Aldrich), 1% penicillin-streptomycin (#15140-122, Gibco, Thermo Fischer Scientific) and 10 ng/ml mouse M-CSF (#14-8983-80, Thermo Fisher Scientific) (M0). Media was exchanged every 2 days. For polarization experiments, cells were seeded in Nunc™ Multidishes with UpCell™ Surface (#174899, Thermo Fischer Scientific) with 10 ng/ml mouse M-CSF for M0 or 10ng/ml

mouse IFNγ (#315-05, Peprotech) plus 10 ng/ml LPS (#L4391, Sigma) for M1. Polarization was done for 24h in the presence or absence of 0.5 µM of Bemcentinib (BergenBio, ASA, Bergen, Norway).

Administration of Antibodies and Liposome Suspension

Clodronate liposomes were purchased from Liposoma Research (Amsterdam, Netherlands) and delivered intravenously (iv) at a dose of 250 µl/mouse as indicated in Fig. legends. All depletion antibodies were purchased from Hölzel Diagnostika (Köln, Germany) and administered *via* i.p injection***. CD8 depletion***: InVivoMab anti-mouse CD8alpha (BE0061) and InVivoMab rat IgG2b isotype control (BE0090) were administered at a dose of 50 µg /mouse. ***NK depletion***: InVivoMab anti-mouse NK1.1 (BE0036) and InVivoMab mouse IgG2a isotype control (BE0085) were diluted in the InVivoPure pH7.0 dilution buffer (Hölzel Diagnostika; IP0070) and administered at a dose of 50 µg /mouse. ***PD1 blockade:*** InVivoMab anti-mouse PD1 (BE0146) and InVivoMab Rat IgG2a isotype control (BE0089) were administered at a dose of 200 µg /mouse every 4 days. Anti-PD1 and Rat IgG2a isotype control antibodies were diluted in the InVivoPure pH7.0 and pH6.5 dilution buffers, respectively, (Hölzel Diagnostika; IP0070) as recommended by the manufacturer. ***IL10, IL12, and TNFα blocking antibodies:*** InVivoMab anti-mouse IL12p40 (BE0051) and anti-mouse TNFα (BE0058) were administered *via* i.p injection at a dose of 300 and 400 µg / mouse/ day, respectively, for the whole duration of the experiment, as indicated in Fig. 6D. IL10 neutralizing antibody (BE0049) or Rat IgG1 isotype control (BE0088) were administered daily at 300 µg /mouse as described I Supplementary Fig. S2M.

Histological Analyses

Tissue samples (spleen, liver, brain and femur) fixed in ROTI® Histofix 4% (#P087.3, Carl Roth), dehydrated and embedded in paraffin. Bones were decalcified in 0.5 M EDTA PH7.4 (#ED2SS, Sigma-Aldrich) at 4°C under constant agitation, for 1-2 weeks, prior to embedding. Paraffin sections (3µm) were subjected to either H&E staining or immunohistochemistry staining on a Leica Bond-Max using the detection systems Bond Polymer Refine Detection (Leica) for anti-rabbit and anti-mouse antibodies or Bond Intense R Detection (Leica) for anti-goat antibodies. Primary antibodies were diluted with the Bond Primary Antibody Diluent (Leica). Anti-human GAS6 (1:100, rabbit polyclonal, HPA008275; Sigma-Aldrich), anti-human

CD10 (1:100, ORG-8941, monoclonal mouse clone 56C6, Novocastra); anti-mouse PD1 (1:200, goat polyclonal, R&D, AF1021), anti-human PDL1 (1:200; rabbit monoclonal, Cell Signaling, 13684). Antigen retrieval was performed within the detection system using a citrate or EDTA (CD10) buffer solution. Anti-GFP (1:1000, polyclonal goat, ab6673; Abcam). Antigen retrieval and a secondary antibody staining were performed within the detection system using an EDTA buffer solution and a biotinylated Rabbit anti-Goat IgG Antibody (BA-5000; Vector Laboratories), respectively. MPO staining was performed using the ready to use Rabbit Polyclonal Antibody (Myeloperoxidase (MPO) Ab-1, #RB-373-R7, Thermo Scientific). Slides were examined with a Zeiss Axio Imager 2 microscope and pictures were taken using the AxioVision SE64 Rel.4.9 software. Analysis depicted in Fig. S2M was carried out using QuPath v0.2.3 digital pathology software (73).

Tissue Preparation, Immunofluorescence Staining and Microscopy

Tissues were fixed in ROTI® Histofix 4% (#P087.3, Carl Roth) for 24 h, then washed in PBS for an additional 24 h before transfer into 30% sucrose (#9097.1, CarlRoth) in PBS until full equilibration. Tissues were then embedded in OCT (# 600001, Weckert Labortechnik) and 5 µm tissue sections were cut at a cryostat (Leica, Wetzlar, Germany). For immunofluorescence staining, frozen tissue sections were thawed, dried for 1 h at room temperature and rehydrated for 30 min in PBS. Subsequently, tissue sections were blocked in 3% BSA (#BSA-50, BiomoL) + 0.1% Triton-X100 (# X100, Sigma Aldrich) in PBS for 1 h at room temperature, followed by incubation with primary antibodies in 1% BSA overnight at 4°C, in a humidified chamber. Primary antibodies were used at the following dilutions: anti-AXL (#AF584, R&D; 1:50); Anti-Phospho AXL(#AF2228, R&D; 1:50); (Anti-GAS6 (#AF986, R&D; 1:50); anti-GFP (#ab13970, Abcam; 1:500); Anti-Iba1 (Rabbit; #019-19741, Wako Chemicals; 1:500), Anti-Iba1 (Goatt; #ab48004, Abcam; 1:200). Fluorophore-conjugated secondary antibodies were used at a dilution of 1:500 in 1% BSA in PBS for 1h at room temperature. Hoechst 33342 (#H3570, Thermo Fisher Scientific) was used to counterstain nuclei at a dilution of 1:2500 prior to covering tissues with Fluoromount™ Aqueous Mounting Medium (#F4680, Sigma Aldrich) and cover slides (#631-0158, VWR). Immunofluorescence was visualized with a Yokogawa CQ1 confocal microscope (Yokogawa, Musashino, Japan) using a 40x objective.

Author Manuscript Published OnlineFirst on June 8, 2021; DOI: 10.1158/2159-8290.CD-20-1378
Author manuscripts have been peer reviewed and accepted for publication but have not yet been edited.

Human Samples and Ethical Compliance

All human specimens were obtained after written informed consent in compliance with the institutional review board at the Faculty of Medicine of the Technical University of Munich. (ethics vote number 538/16) and the university hospital Carl Gustav Carus (ethics vote number EK49022018). Paraffin embedded bone marrow trephine biopsies were retrieved from archived diagnostic samples (Patient information is presented in Table S1). The medical chart of all patients was reviewed by a physician to confirm the diagnosis and clinical data. Evaluation of GAS6 staining on bone marrow biopsies was carried out by a trained pathologist. Pseudonymized use of healthy donor buffy coat preparations from whole blood donations was approved by the Ethics Committee of Goethe University of Medicine, under ethics vote 329/10.

QUANTIFICATION AND STATISTICAL ANALYSIS

All statistical analyses were carried out using version 7 of the GraphPad Prism software. Kaplan-Meier survival curves with two-sided log-rank Mantel-cox analysis was used to evaluate the difference in survival *in vivo*. Comparison of leukemic burdens and target expression levels were carried out using two-sided Student's t-tests.

DATA AND CODE AVAILABILITY

All raw sequencing data have been deposited in the European Nucleotide Archive (https://www.ebi.ac.uk/ena/) under the accession number: PRJEB43830. Further information and requests for resources and reagents may be directed to and will be fulfilled by the Lead Contact, Hind Medyouf (Medyouf@gsh.uni-frankfurt.de). All unique/stable reagents generated in this study are available from the Lead Contact with a completed Materials Transfer Agreement.

References

1. Bassan R, Bourquin JP, DeAngelo DJ, Chiaretti S. New Approaches to the Management of Adult Acute Lymphoblastic Leukemia. J Clin Oncol **2018**:JCO2017773648 doi 10.1200/JCO.2017.77.3648.
2. Dohner H, Weisdorf DJ, Bloomfield CD. Acute Myeloid Leukemia. N Engl J Med **2015**;373(12):1136-52 doi 10.1056/NEJMra1406184.
3. Witkowski MT, Lasry A, Carroll WL, Aifantis I. Immune-Based Therapies in Acute Leukemia. Trends Cancer **2019**;5(10):604-18 doi 10.1016/j.trecan.2019.07.009.
4. Christopher MJ, Petti AA, Rettig MP, Miller CA, Chendamarai E, Duncavage EJ*, et al.* Immune Escape of Relapsed AML Cells after Allogeneic Transplantation. N Engl J Med **2018**;379(24):2330-41 doi 10.1056/NEJMoa1808777.
5. Toffalori C, Zito L, Gambacorta V, Riba M, Oliveira G, Bucci G*, et al.* Immune signature drives leukemia escape and relapse after hematopoietic cell transplantation. Nat Med **2019**;25(4):603-11 doi 10.1038/s41591-019-0400-z.
6. Vago L, Perna SK, Zanussi M, Mazzi B, Barlassina C, Stanghellini MT*, et al.* Loss of mismatched HLA in leukemia after stem-cell transplantation. N Engl J Med **2009**;361(5):478-88 doi 10.1056/NEJMoa0811036.
7. Giannopoulos K. Targeting Immune Signaling Checkpoints in Acute Myeloid Leukemia. J Clin Med **2019**;8(2) doi 10.3390/jcm8020236.
8. Paczulla AM, Rothfelder K, Raffel S, Konantz M, Steinbacher J, Wang H*, et al.* Absence of NKG2D ligands defines leukaemia stem cells and mediates their immune evasion. Nature **2019**;572(7768):254-9 doi 10.1038/s41586-019-1410-1.
9. Alexandrov LB, Nik-Zainal S, Wedge DC, Aparicio SA, Behjati S, Biankin AV*, et al.* Signatures of mutational processes in human cancer. Nature **2013**;500(7463):415-21 doi 10.1038/nature12477.
10. Curran EK, Godfrey J, Kline J. Mechanisms of Immune Tolerance in Leukemia and Lymphoma. Trends in immunology **2017**;38(7):513-25 doi 10.1016/j.it.2017.04.004.
11. Curran E, Chen X, Corrales L, Kline DE, Dubensky TW, Jr., Duttagupta P*, et al.* STING Pathway Activation Stimulates Potent Immunity against Acute Myeloid Leukemia. Cell reports **2016**;15(11):2357-66 doi 10.1016/j.celrep.2016.05.023.
12. Engblom C, Pfirschke C, Pittet MJ. The role of myeloid cells in cancer therapies. Nature reviews Cancer **2016**;16(7):447-62 doi 10.1038/nrc.2016.54.
13. Witkowski MT, Dolgalev I, Evensen NA, Ma C, Chambers T, Roberts KG*, et al.* Extensive Remodeling of the Immune Microenvironment in B Cell Acute Lymphoblastic Leukemia. Cancer Cell **2020**;37(6):867-82 e12 doi 10.1016/j.ccell.2020.04.015.
14. Komohara Y, Niino D, Saito Y, Ohnishi K, Horlad H, Ohshima K*, et al.* Clinical significance of CD163(+) tumor-associated macrophages in patients with adult T-cell leukemia/lymphoma. Cancer Sci **2013**;104(7):945-51 doi 10.1111/cas.12167.
15. van Galen P, Hovestadt V, Wadsworth Ii MH, Hughes TK, Griffin GK, Battaglia S*, et al.* Single-Cell RNA-Seq Reveals AML Hierarchies Relevant to Disease Progression and Immunity. Cell **2019**;176(6):1265-81 e24 doi 10.1016/j.cell.2019.01.031.
16. Lumbroso D, Soboh S, Maimon A, Schif-Zuck S, Ariel A, Burstyn-Cohen T. Macrophage-Derived Protein S Facilitates Apoptotic Polymorphonuclear Cell Clearance by Resolution Phase Macrophages and Supports Their Reprogramming. Front Immunol **2018**;9:358 doi 10.3389/fimmu.2018.00358.
17. Bosurgi L, Hughes LD, Rothlin CV, Ghosh S. Death begets a new beginning. Immunol Rev **2017**;280(1):8-25 doi 10.1111/imr.12585.

18. Rothlin CV, Carrera-Silva EA, Bosurgi L, Ghosh S. TAM receptor signaling in immune homeostasis. Annu Rev Immunol **2015**;33:355-91 doi 10.1146/annurev-immunol-032414-112103.
19. Gay CM, Balaji K, Byers LA. Giving AXL the axe: targeting AXL in human malignancy. British journal of cancer **2017**;116(4):415-23 doi 10.1038/bjc.2016.428.
20. Graham DK, DeRyckere D, Davies KD, Earp HS. The TAM family: phosphatidylserine sensing receptor tyrosine kinases gone awry in cancer. Nature reviews Cancer **2014**;14(12):769-85 doi 10.1038/nrc3847.
21. Ben-Batalla I, Erdmann R, Jorgensen H, Mitchell R, Ernst T, von Amsberg G*, et al.* Axl Blockade by BGB324 Inhibits BCR-ABL Tyrosine Kinase Inhibitor-Sensitive and -Resistant Chronic Myeloid Leukemia. Clinical cancer research : an official journal of the American Association for Cancer Research **2017**;23(9):2289-300 doi 10.1158/1078-0432.CCR-16-1930.
22. Ben-Batalla I, Schultze A, Wroblewski M, Erdmann R, Heuser M, Waizenegger JS*, et al.* Axl, a prognostic and therapeutic target in acute myeloid leukemia mediates paracrine crosstalk of leukemia cells with bone marrow stroma. Blood **2013**;122(14):2443-52 doi 10.1182/blood-2013-03-491431.
23. Brandao LN, Winges A, Christoph S, Sather S, Migdall-Wilson J, Schlegel J*, et al.* Inhibition of MerTK increases chemosensitivity and decreases oncogenic potential in T-cell acute lymphoblastic leukemia. Blood cancer journal **2013**;3:e101 doi 10.1038/bcj.2012.46.
24. Jin Y, Nie D, Li J, Du X, Lu Y, Li Y*, et al.* Gas6/AXL Signaling Regulates Self-Renewal of Chronic Myelogenous Leukemia Stem Cells by Stabilizing beta-Catenin. Clinical cancer research : an official journal of the American Association for Cancer Research **2017**;23(11):2842-55 doi 10.1158/1078-0432.CCR-16-1298.
25. Lee-Sherick AB, Eisenman KM, Sather S, McGranahan A, Armistead PM, McGary CS*, et al.* Aberrant Mer receptor tyrosine kinase expression contributes to leukemogenesis in acute myeloid leukemia. Oncogene **2013**;32(46):5359-68 doi 10.1038/onc.2013.40.
26. Park IK, Mundy-Bosse B, Whitman SP, Zhang X, Warner SL, Bearss DJ*, et al.* Receptor tyrosine kinase Axl is required for resistance of leukemic cells to FLT3-targeted therapy in acute myeloid leukemia. Leukemia **2015**;29(12):2382-9 doi 10.1038/leu.2015.147.
27. Sinha S, Boysen J, Nelson M, Warner SL, Bearss D, Kay NE*, et al.* Axl activates fibroblast growth factor receptor pathway to potentiate survival signals in B-cell chronic lymphocytic leukemia cells. Leukemia **2016**;30(6):1431-6 doi 10.1038/leu.2015.323.
28. Whitman SP, Kohlschmidt J, Maharry K, Volinia S, Mrozek K, Nicolet D*, et al.* GAS6 expression identifies high-risk adult AML patients: potential implications for therapy. Leukemia **2014**;28(6):1252-8 doi 10.1038/leu.2013.371.
29. Niu X, Rothe K, Chen M, Grasedieck S, Li R, Nam SE*, et al.* Targeting AXL Kinase Sensitizes Leukemic Stem and Progenitor Cells to Venetoclax Treatment in Acute Myeloid Leukemia. Blood **2021** doi 10.1182/blood.2020007651.
30. Aguilera TA, Rafat M, Castellini L, Shehade H, Kariolis MS, Hui AB*, et al.* Reprogramming the immunological microenvironment through radiation and targeting Axl. Nat Commun **2016**;7:13898 doi 10.1038/ncomms13898.

31. Tsukita Y, Fujino N, Miyauchi E, Saito R, Fujishima F, Itakura K*, et al.* Axl kinase drives immune checkpoint and chemokine signalling pathways in lung adenocarcinomas. Mol Cancer **2019**;18(1):24 doi 10.1186/s12943-019-0953-y.
32. Terry S, Abdou A, Engelsen AST, Buart S, Dessen P, Corgnac S*, et al.* AXL Targeting Overcomes Human Lung Cancer Cell Resistance to NK- and CTL-Mediated Cytotoxicity. Cancer Immunol Res **2019**;7(11):1789-802 doi 10.1158/2326-6066.CIR-18-0903.
33. Skinner HD, Giri U, Yang LP, Kumar M, Liu Y, Story MD*, et al.* Integrative Analysis Identifies a Novel AXL-PI3 Kinase-PD-L1 Signaling Axis Associated with Radiation Resistance in Head and Neck Cancer. Clinical cancer research : an official journal of the American Association for Cancer Research **2017**;23(11):2713-22 doi 10.1158/1078-0432.CCR-16-2586.
34. Sadahiro H, Kang KD, Gibson JT, Minata M, Yu H, Shi J*, et al.* Activation of the Receptor Tyrosine Kinase AXL Regulates the Immune Microenvironment in Glioblastoma. Cancer Res **2018**;78(11):3002-13 doi 10.1158/0008-5472.CAN-17-2433.
35. Ludwig KF, Du W, Sorrelle NB, Wnuk-Lipinska K, Topalovski M, Toombs JE*, et al.* Small-Molecule Inhibition of Axl Targets Tumor Immune Suppression and Enhances Chemotherapy in Pancreatic Cancer. Cancer Res **2018**;78(1):246-55 doi 10.1158/0008-5472.CAN-17-1973.
36. Hugo W, Zaretsky JM, Sun L, Song C, Moreno BH, Hu-Lieskovan S*, et al.* Genomic and Transcriptomic Features of Response to Anti-PD-1 Therapy in Metastatic Melanoma. Cell **2016**;165(1):35-44 doi 10.1016/j.cell.2016.02.065.
37. Abdel-Wahab O, Gao J, Adli M, Dey A, Trimarchi T, Chung YR*, et al.* Deletion of Asxl1 results in myelodysplasia and severe developmental defects in vivo. The Journal of experimental medicine **2013**;210(12):2641-59 doi 10.1084/jem.20131141.
38. Horton SJ, Walf-Vorderwulbecke V, Chatters SJ, Sebire NJ, de Boer J, Williams O. Acute myeloid leukemia induced by MLL-ENL is cured by oncogene ablation despite acquisition of complex genetic abnormalities. Blood **2009**;113(20):4922-9 doi 10.1182/blood-2008-07-170480.
39. Pfeifer H, Raum K, Markovic S, Nowak V, Fey S, Oblander J*, et al.* Genomic CDKN2A/2B deletions in adult Ph(+) ALL are adverse despite allogeneic stem cell transplantation. Blood **2018**;131(13):1464-75 doi 10.1182/blood-2017-07-796862.
40. Waizenegger JS, Ben-Batalla I, Weinhold N, Meissner T, Wroblewski M, Janning M*, et al.* Role of Growth arrest-specific gene 6-Mer axis in multiple myeloma. Leukemia **2015**;29(3):696-704 doi 10.1038/leu.2014.236.
41. Nepal S, Tiruppathi C, Tsukasaki Y, Farahany J, Mittal M, Rehman J*, et al.* STAT6 induces expression of Gas6 in macrophages to clear apoptotic neutrophils and resolve inflammation. Proc Natl Acad Sci U S A **2019**;116(33):16513-8 doi 10.1073/pnas.1821601116.
42. Bosurgi L, Cao YG, Cabeza-Cabrerizo M, Tucci A, Hughes LD, Kong Y*, et al.* Macrophage function in tissue repair and remodeling requires IL-4 or IL-13 with apoptotic cells. Science **2017**;356(6342):1072-6 doi 10.1126/science.aai8132.
43. Gokbuget N. Treatment of older patients with acute lymphoblastic leukemia. Hematology Am Soc Hematol Educ Program **2016**;2016(1):573-9 doi 10.1182/asheducation-2016.1.573.
44. Vignetti M, Fazi P, Cimino G, Martinelli G, Di Raimondo F, Ferrara F*, et al.* Imatinib plus steroids induces complete remissions and prolonged survival in elderly

Philadelphia chromosome-positive patients with acute lymphoblastic leukemia without additional chemotherapy: results of the Gruppo Italiano Malattie Ematologiche dell'Adulto (GIMEMA) LAL0201-B protocol. Blood **2007**;109(9):3676-8 doi 10.1182/blood-2006-10-052746.

45. Heng TS, Painter MW, Immunological Genome Project C. The Immunological Genome Project: networks of gene expression in immune cells. Nature immunology **2008**;9(10):1091-4 doi 10.1038/ni1008-1091.
46. Ubil E, Caskey L, Holtzhausen A, Hunter D, Story C, Earp HS. Tumor-secreted Pros1 inhibits macrophage M1 polarization to reduce antitumor immune response. The Journal of clinical investigation **2018**;128(6):2356-69 doi 10.1172/JCI97354.
47. Maier B, Leader AM, Chen ST, Tung N, Chang C, LeBerichel J*, et al.* A conserved dendritic-cell regulatory program limits antitumour immunity. Nature **2020**;580(7802):257-62 doi 10.1038/s41586-020-2134-y.
48. Schmid ET, Pang IK, Carrera Silva EA, Bosurgi L, Miner JJ, Diamond MS*, et al.* AXL receptor tyrosine kinase is required for T cell priming and antiviral immunity. Elife **2016**;5 doi 10.7554/eLife.12414.
49. Xu K, Harrison RE. Down-regulation of Stathmin Is Required for the Phenotypic Changes and Classical Activation of Macrophages. J Biol Chem **2015**;290(31):19245-60 doi 10.1074/jbc.M115.639625.
50. Mantovani A, Sica A, Sozzani S, Allavena P, Vecchi A, Locati M. The chemokine system in diverse forms of macrophage activation and polarization. Trends in immunology **2004**;25(12):677-86 doi 10.1016/j.it.2004.09.015.
51. Balkwill F. Tumour necrosis factor and cancer. Nature reviews Cancer **2009**;9(5):361-71 doi 10.1038/nrc2628.
52. Tugues S, Burkhard SH, Ohs I, Vrohlings M, Nussbaum K, Vom Berg J*, et al.* New insights into IL-12-mediated tumor suppression. Cell Death Differ **2015**;22(2):237-46 doi 10.1038/cdd.2014.134.
53. Murray PJ. Macrophage Polarization. Annu Rev Physiol **2017**;79:541-66 doi 10.1146/annurev-physiol-022516-034339.
54. Merad M, Sathe P, Helft J, Miller J, Mortha A. The dendritic cell lineage: ontogeny and function of dendritic cells and their subsets in the steady state and the inflamed setting. Annu Rev Immunol **2013**;31:563-604 doi 10.1146/annurev-immunol-020711-074950.
55. Zhou Y, Fei M, Zhang G, Liang WC, Lin W, Wu Y*, et al.* Blockade of the Phagocytic Receptor MerTK on Tumor-Associated Macrophages Enhances P2X7R-Dependent STING Activation by Tumor-Derived cGAMP. Immunity **2020**;52(2):357-73 e9 doi 10.1016/j.immuni.2020.01.014.
56. Holland SJ, Pan A, Franci C, Hu Y, Chang B, Li W*, et al.* R428, a selective small molecule inhibitor of Axl kinase, blocks tumor spread and prolongs survival in models of metastatic breast cancer. Cancer Res **2010**;70(4):1544-54 doi 10.1158/0008-5472.CAN-09-2997.
57. Yang X, Shi J, Zhang X, Zhang G, Zhang J, Yang S*, et al.* ssExpression level of GAS6-mRNA influences the prognosis of acute myeloid leukemia patients with allogeneic hematopoietic stem cell transplantation. Biosci Rep **2019**;39(5) doi 10.1042/BSR20190389.
58. Kaczanowska S, Beury DW, Gopalan V, Tycko AK, Qin H, Clements ME*, et al.* Genetically engineered myeloid cells rebalance the core immune suppression program in metastasis. Cell **2021**;184(8):2033-52 e21 doi 10.1016/j.cell.2021.02.048.

59. Chen DS, Mellman I. Oncology meets immunology: the cancer-immunity cycle. Immunity **2013**;39(1):1-10 doi 10.1016/j.immuni.2013.07.012.
60. Lu Q, Lemke G. Homeostatic regulation of the immune system by receptor tyrosine kinases of the Tyro 3 family. Science **2001**;293(5528):306-11 doi 10.1126/science.1061663.
61. Loges S, Heuser M, Chromik J, Vigil CE, Paschka P, Ben-Batalla I*, et al.* Final Analysis of the Dose Escalation, Expansion and Biomarker Correlations in the Ph I/II Trial BGBC003 with the Selective Oral AXL Inhibitor Bemcentinib (BGB324) in Relapsed/Refractory AML and MDS. Blood **2018**;132(Supplement 1):2672- doi 10.1182/blood-2018-99-120380.
62. Perl AE, Martinelli G, Cortes JE, Neubauer A, Berman E, Paolini S*, et al.* Gilteritinib or Chemotherapy for Relapsed or Refractory FLT3-Mutated AML. N Engl J Med **2019**;381(18):1728-40 doi 10.1056/NEJMoa1902688.
63. Tirado-Gonzalez I, Czlonka E, Nevmerzhitskaya A, Soetopo D, Bergonzani E, Mahmoud A*, et al.* CRISPR/Cas9-edited NSG mice as PDX models of human leukemia to address the role of niche-derived SPARC. Leukemia **2018**;32(4):1049-52 doi 10.1038/leu.2017.346.
64. Morita S, Kojima T, Kitamura T. Plat-E: an efficient and stable system for transient packaging of retroviruses. Gene Ther **2000**;7(12):1063-6 doi 10.1038/sj.gt.3301206.
65. Medyouf H, Alcalde H, Berthier C, Guillemin MC, dos Santos NR, Janin A*, et al.* Targeting calcineurin activation as a therapeutic strategy for T-cell acute lymphoblastic leukemia. Nat Med **2007**;13(6):736-41 doi 10.1038/nm1588.
66. Passaro D, Di Tullio A, Abarrategi A, Rouault-Pierre K, Foster K, Ariza-McNaughton L*, et al.* Increased Vascular Permeability in the Bone Marrow Microenvironment Contributes to Disease Progression and Drug Response in Acute Myeloid Leukemia. Cancer Cell **2017**;32(3):324-41 e6 doi 10.1016/j.ccell.2017.08.001.
67. Cancer Genome Atlas Research N, Ley TJ, Miller C, Ding L, Raphael BJ, Mungall AJ*, et al.* Genomic and epigenomic landscapes of adult de novo acute myeloid leukemia. N Engl J Med **2013**;368(22):2059-74 doi 10.1056/NEJMoa1301689.
68. Aguirre-Gamboa R, Gomez-Rueda H, Martinez-Ledesma E, Martinez-Torteya A, Chacolla-Huaringa R, Rodriguez-Barrientos A*, et al.* SurvExpress: an online biomarker validation tool and database for cancer gene expression data using survival analysis. PLoS One **2013**;8(9):e74250 doi 10.1371/journal.pone.0074250.
69. Stuart T, Butler A, Hoffman P, Hafemeister C, Papalexi E, Mauck WM, 3rd*, et al.* Comprehensive Integration of Single-Cell Data. Cell **2019**;177(7):1888-902 e21 doi 10.1016/j.cell.2019.05.031.
70. Diaz-Papkovich A, Anderson-Trocme L, Ben-Eghan C, Gravel S. UMAP reveals cryptic population structure and phenotype heterogeneity in large genomic cohorts. PLoS Genet **2019**;15(11):e1008432 doi 10.1371/journal.pgen.1008432.
71. Finak G, McDavid A, Yajima M, Deng J, Gersuk V, Shalek AK*, et al.* MAST: a flexible statistical framework for assessing transcriptional changes and characterizing heterogeneity in single-cell RNA sequencing data. Genome Biol **2015**;16:278 doi 10.1186/s13059-015-0844-5.
72. Wolf A, Couttet P, Dong M, Grenet O, Heron M, Junker U*, et al.* Preclinical evaluation of potential nilotinib cardiotoxicity. Leuk Res **2011**;35(5):631-7 doi 10.1016/j.leukres.2010.11.001.

73. Bankhead P, Loughrey MB, Fernandez JA, Dombrowski Y, McArt DG, Dunne PD*, et al.* QuPath: Open source software for digital pathology image analysis. Sci Rep **2017**;7(1):16878 doi 10.1038/s41598-017-17204-5.

Figure 1. Leukemia-induced GAS6 contributes to immune evasion and leukemic progression.

(**A**) Prognostic value of *GAS6* expression in acute myeloid leukemia (TCGA LAML, n=173). Data was generated using the KaplanScan mode from the R2 Genomics Analysis and Visualization Platform (http://r2.amc.nl). Survival analysis by log-rank (Mantel–Cox) test.

(**B**) Immunohistochemistry (IHC) of GAS6 on bone marrow trephine biopsies from representative Ph+ (BCR-ABL1$^+$) B-ALL patients at diagnosis. CD10 marks B-ALL blasts (upper left). Arrowhead marks myeloid cells; asterisks marks megakaryocytes; white pyramids marks vessels/serum.

(**C**) CD14$^+$ peripheral blood monocytes from healthy donors were cultured with leukemia cells from either Ph+ B-ALL patients (Left: CD14$^+$ from 11 donors cultured with 2 Ph$^+$ B-ALL) or patients with myeloid diseases (right: CD14$^+$ from 8 donors cultured with 1 AML and 1 higher-risk myelodysplatic syndrome). Then GAS6 mRNA levels was determined by real-time PCR. Each data point represents a mean value obtained from 2 technical replicates, after normalization to a reference gene, *GUSB*. **p<0.01, paired two-tailed Student's *t*-test. Characteristics of all patients and healthy donors are described in Table S1.

(**D, E and F**) WT and *Gas6*$^{-/-}$ C57BL/6 or NSG (NSG *Gas6*$^{-/-}$, line$^{\#697\text{-}31}$) mice were challenged with *Asxl1*$^{-/-}$ leukemia cells (10^5). Weight of spleens and livers on day 19 days post-leukemia challenge are displayed. NSG (n= 5) and C57BL/6 (n = 6) mice without leukemia are used as reference. ns, not significant. ***p<0.001, paired two-tailed Student's *t*-test.

(**G**) Kaplan–Meier survival analysis of WT and *Gas6*$^{-/-}$ C57BL/6 challenged with *Asxl1*$^{-/-}$ leukemia cells (10^5). **p<0.01, log-rank (Mantel–Cox) test.

(**H, I and J**) WT and *Gas6*$^{-/-}$ C57BL/6 or NSG (NSG *Gas6*$^{-/-}$, line$^{\#697\text{-}31}$) mice were challenged with MLL-ENL AML cells (10^5). BM aspiration was performed after 22-days to determine leukemic burden (Tomato$^+$). ns, not significant. *, p<0.05, paired two-tailed Student's *t*-test.

(**K**) Kaplan–Meier survival analysis of WT and *Gas6*$^{-/-}$ C57BL/6 challenged with MLL-ENL AML cells (10^5). **p<0.01, log-rank (Mantel–Cox) test.

(**L, M and N**) WT and *Gas6*$^{-/-}$ C57BL/6 or NSG (NSG *Gas6*$^{-/-}$, line$^{\#697\text{-}29}$) mice were challenged with B-ALL cells (10^3) and analyzed two weeks post leukemia injection for leukemic burden (B220$^+$GFP$^+$) in bone marrow (BM), spleen (Spl) and peripheral blood (PB). This experiment was repeated with a different NSG *Gas6*$^{-/-}$ mouse line (line$^{\#697\text{-}31}$) with similar results (Figure S3E). ns, not significant. ***p<0.001, paired two-tailed Student's *t*-test.

(**O**) Kaplan–Meier survival analysis of WT and *Gas6*$^{-/-}$ C57BL/6 challenged with B-ALL cells (10^3). ns, not significant, log-rank (Mantel–Cox) test.

(**P and Q**) Kaplan–Meier survival analysis of WT and *Gas6*$^{-/-}$ C57BL/6 challenged with B-ALL cells (10^3) and subjected to either vehicle or nilotinib plus vincristine treatment combination. Treatment was initiated on day 7 and terminated on day 39. Data representative of at least 2 independent experiments. *p<0.05, ***p<0.001, log-rank (Mantel–Cox) test.

Author Manuscript Published OnlineFirst on June 8, 2021; DOI: 10.1158/2159-8290.CD-20-1378
Author manuscripts have been peer reviewed and accepted for publication but have not yet been edited.

Figure 2. Selective *Axl* ablation in macrophages confers effective protection against leukemia.

(**A**) Representative immune fluorescence showing AXL expression (White) in Iba1$^+$ leukemia-associated macrophages (Red) in the spleen of a B-ALL leukemia bearing mouse.

(**B**) leukemic burden (% of GFP$^+$ B220$^+$) in bone marrow (BM), spleen (Spl) and peripheral blood (PB) of *Axl$^{f/f}$* (n = 6) and *Csf1r-Cre$^+$ Axl$^{f/f}$* (n = 4) animals twelve days after challenge with 10^3 B-ALL cells. ***p<0.001, unpaired two-tailed Student's *t*-test. Experiment is representative of at least three experiments.

(**C**) Kaplan–Meier survival analysis of control *Axl$^{f/f}$* and *Csf1r-Cre$^+$ Axl$^{f/f}$* animals challenged with 10^3 Ph$^+$ B-ALL. Data are from 2 independent experiments. Similar results obtained in a third experiment using a different primary B-ALL. ****p<0.0001, log-rank (Mantel–Cox) test.

(**D**) leukemic burden (% of GFP$^+$ B220$^+$) in BM, Spl and PB of *Axl$^{f/f}$* (n = 4) and *CD11c-Cre$^+$* (*CD11c-eGFP-Cre$^+$ Axl$^{f/f}$,* n = 3) mice twelve days after challenge with 10^3 B-ALL cells**.** ns, not significant, unpaired two-tailed Student's *t*-test. Experiment is representative of 2 independent experiments.

(**E**)**,** *Csf1r-Cre$^+$* control mice (n = 5) and *Csf1r-Cre$^+$ Axl$^{f/f}$* mice (n = 4) received 1 injection of clodronate liposomes (250ul i.v / mouse) 3 days before challenge with 10^3 B-ALL cells. Three weeks later, when the first mouse was terminally ill, all mice were sacrificed and leukemic burden evaluated in BM, Spl and PB. ns, not significant, unpaired two-tailed Student's *t*-test.

(**F**) *Axl$^{f/f}$* (n = 3) and *Csf1r-Cre$^+$ Axl$^{f/f}$* (n = 3) animals were challenged with 5.10^5 *Asxl1$^{-/-}$* AML cells. At day 26, leukemic burden (CD11b^{dim}B220^{dim}) in BM, Spl and PB is depicted. **p<0.01, unpaired two-tailed Student's *t*-test.

(**G**)**,** Kaplan–Meier survival analysis of control *Axl$^{f/f}$* (n = 9) and *Csf1r-Cre$^+$ Axl$^{f/f}$* (n = 6) animals challenged with 10^5 *Asxl1$^{-/-}$* AML as in (F). **p<0.01, log-rank (Mantel–Cox) test.

(**H**) *Axl$^{f/f}$* (n = 4) and *Csf1r-Cre$^+$ Axl$^{f/f}$* (n = 4) animals were challenged with 10^5 *MLL-ENL* AML cells. At day 28, leukemic burden (% tomato$^+$ CD11b$^+$) in BM, Spl and PB is depicted. ***p<0.001, unpaired two-tailed Student's *t*-test.

(**I**) Kaplan–Meier survival analysis of control *Axl$^{f/f}$* and *Csf1r-Cre$^+$ Axl$^{f/f}$* animals challenged with 10^5 MLL-ENL AML. These mice are also depicted in Figure 4I. **p<0.01, log-rank (Mantel–Cox) test.

(**J**) *Axl$^{f/f}$* (n = 8) and *CD11c-Cre$^+$* (*CD11c-eGFP-Cre$^+$ Axl$^{f/f}$,* n = 6) mice were challenged with 10^5 *MLL-ENL* AML. On day 26, leukemic burden (% tomato$^+$ CD11b$^+$) in BM, Spl and PB is depicted. ns, not significant, unpaired two-tailed Student's *t*-test.

Author Manuscript Published OnlineFirst on June 8, 2021; DOI: 10.1158/2159-8290.CD-20-1378
Author manuscripts have been peer reviewed and accepted for publication but have not yet been edited.

Figure 3. *Axl*-deficient macrophages prevent the establishment of an immune suppressive environment in response to leukemia.

(**A**) Non-leukemic (GFP$^-$) spleen leukocytes were FACS purified from control *Axl*$^{f/f}$ mice and *Csf1r-Cre*$^+$ *Axl*$^{f/f}$ mice that were either naïve (*Axl*$^{f/f}$ *n = 2; Csf1r-Cre*$^+$ *Axl*$^{f/f}$ n = 2*)* or challenged with 10^3 B-ALL cells (n = 2 *Axl*$^{f/f}$ + B-ALL; n = 2 *Csf1r-Cre*$^+$ *Axl*$^{f/f}$+ B-ALL) for 8 days and subjected to 10X Genomics scRNA sequencing. Data clustering, UMAP visualization of 36000 individual cells (pooled from all conditions) followed by marker-based cell type annotation identified 10 broad immune subsets across all profiled single cells.

(**B**) Dot plot of selected cluster specific marker genes**.**

(**C**) Relative abundance of identified cell types across conditions.

(**D)** Volcano plots showing the DEG (Padj<0.01 and fold change >1.5) in macrophages comparing *Axl*$^{f/f}$ and *Csf1r-Cre*$^+$ *Axl*$^{f/f}$ under steady state conditions (left) and upon leukemia challenge (right), with the significant genes (max 10) annotated.

(**E**) Real-time PCR expression data in F4/80$^+$ spleen macrophages purified using magnetic beads from naïve WT mice (n = 4) and mice transplanted with 10^3 B-ALL (WT n = 4; *Csf1r-Cre*$^+$ *Axl*$^{f/f}$ n = 4). Data are normalized to a reference gene, *Ubc* and are mean ± s.e.m. *p<0.05, unpaired two-tailed Student's *t*-test.

(F) Real-time PCR expression data in dendritic cells (DCs) isolated by flow cytometry as CD45$^+$GFP$^-$MHC-II$^+$CD11c$^+$ from the spleen of B-ALL challenged *Axl*$^{f/f}$ (n = 4) and *Csf1r-Cre*$^+$ *Axl*$^{f/f}$ mice (n = 3). Data are normalized to a reference gene, *Sdha* and are mean ± s.e.m. *p<0.05, ****p<0.0001, unpaired two-tailed Student's *t*-test.

(G) Representative gating and flow cytometry based quantification of total classical dendritic cells (DCs: CD45$^+$GFP$^-$MHC-II$^+$CD11c$^+$) as well as subsets: cDC1 (CD8$^+$DCs: MHC-II$^+$CD11c$^+$CD8$^+$CD11b$^-$) and cDC2 (CD11b$^+$DCs: MHC-II$^+$CD11c$^+$CD8$^-$CD11b$^+$) within non-leukemic splenocytes (GFP$^-$CD45$^+$) from B-ALL challenged *Axl*$^{f/f}$ (n = 6) and *Csf1r-Cre*$^+$ *Axl*$^{f/f}$ (n = 4) mice. ns, not significant, ***p<0.001, unpaired two-tailed Student's *t*-test.

Author Manuscript Published OnlineFirst on June 8, 2021; DOI: 10.1158/2159-8290.CD-20-1378
Author manuscripts have been peer reviewed and accepted for publication but have not yet been edited.

Figure 4. *Axl* deficient macrophages trigger a robust NK- and T cell immune response that suppresses leukemia.

(**A and B**) *Axl*$^{f/f}$ *and Csf1r-Cre*$^{+}$ *Axl*$^{f/f}$ mice were challenged with 10^3 B-ALL cells and treated with either an anti-NK1.1 antibody or a mouse IgG2a isotype control (50 µg /mouse) every 5 days as indicated. Leukemic burden (% GFP^{+}) in the BM and Spl on day 14 is depicted (B). ns, not significant. ***p<0.001, unpaired two-tailed Student's *t*-test.

(**C**) Kaplan-Meier survival analysis of mice of the indicated genotypes challenged with 10^3 B-ALL cells and treated as in A. Treatments stopped once all anti-NK1.1 treated mice were dead. ns, not significant. **p<0.01, log-rank (Mantel–Cox) test.

(**D, E**) Same as in A-B using 10^5 *MLL-ENL* AML cells. Leukemic burden (% Tomato^{+}) on day 25 is depicted. ns, not significant. **p<0.01, ***p<0.001, unpaired two-tailed Student's *t*-test.

(**F**) Kaplan-Meier survival analysis of mice of the indicated genotypes challenged with 10^5 *MLL-ENL* AML cells and treated as in D. Treatments stopped once all anti NK1.1 treated mice were dead. ns, not significant. **p<0.01, ***p<0.001, log-rank (Mantel–Cox) test.

(**G**) Kaplan-Meier survival analysis of mice of the indicated genotypes challenged with 10^3 B-ALL cells. Data are pooled from two independent experiments as indicated in the scheme. **p<0.01, ***p<0.001, ****p<0.0001, log-rank (Mantel–Cox) test.

(**H**) Leukemic burden (% GFP+) in all terminally ill animals that could be analyzed from G**.** Note that burden from animals found dead cannot be depicted. ns, not significant. *p<0.05, **p<0.01, unpaired two-tailed Student's *t*-test.

(**I**) Kaplan-Meier survival curve of mice of the indicated genotypes challenged with 10^5 MLL-ENL cells. Survival of the reference groups (*Axl*$^{f/f}$ and *Csf1r-Cre*$^{+}$ *Axl*$^{f/f}$) is also depicted in figure 2I. ns, not significant. **p<0.01, ***p<0.001, log-rank (Mantel–Cox) test.

(**J**) Leukemic burden (% tomato^{+}) in all terminally ill animals that could be analyzed from I. Note that burden from animals found dead cannot be depicted. ns, not significant, unpaired two-tailed Student's *t*-test.

Author Manuscript Published OnlineFirst on June 8, 2021; DOI: 10.1158/2159-8290.CD-20-1378
Author manuscripts have been peer reviewed and accepted for publication but have not yet been edited.

Figure 5. *Axl* deficient macrophages trigger anti-leukemic immunity and elicit PD1 checkpoint blockade.

(**A**) Kaplan–Meier survival analysis of WT mice challenged with 10^3 B-ALL cells and treated with either anti-PD1 (n= 8) or isotype control (n = 7).

(**B**) GFP^+ blasts (left) and $PD1^+$ cells (right) by IHC in the spleen of *Csf1r-Cre*$^+$ *Axl*$^{f/f}$ mice that succumbed to B-ALL with a delayed latency of >40 days (Mice depicted in Figure 2C).

(**C and D**) *Csf1r-Cre*$^+$ *Axl*$^{f/f}$ from 3 independent experiments were followed by weekly bleeding to identify mice with late disease recurrence (n=7). Flow cytometry data depicting PD1 expression in peripheral blood lymphocytes (CD4 and CD8 T cells, NK cells) and corresponding PD1 mean fluorescence intensity (MFI) from *Csf1r-Cre*$^+$ *Axl*$^{f/f}$ mice showing signs of relapse (detectable GFP^+ cells, representative data in G). ****p<0.0001, unpaired two-tailed Student's *t*-test.

(**E**) PD-1 ligand (PDL1) expression by IHC in bone marrow cells with both stromal and hematopoietic morphology (left), as well as on cytospined B-ALL cells (right).

(**F and G**) *Csf1r-Cre*$^+$ *Axl*$^{f/f}$ mice with late disease recurrence (n = 7, depicted in C and D) were either left untreated (n = 3) or subjected to 7 cycles of anti-PD1 treatment (n = 4; 200 µg /mouse every 4 days). Representative FACS plot depicting leukemic burden (GFP^+ $B220^{dim}$) in the peripheral blood of the same mouse before and after one shot of anti-PD1 treatment.

(**H**) Kaplan–Meier survival analysis of mice from F. *p<0.05, log-rank (Mantel–Cox) test.

Author Manuscript Published OnlineFirst on June 8, 2021; DOI: 10.1158/2159-8290.CD-20-1378
Author manuscripts have been peer reviewed and accepted for publication but have not yet been edited.

Figure 6. Bemcentinib, a clinical grade AXL inhibitor triggers effective anti-leukemic immunity in B-ALL that depends on IL12, TNFa and engagement of CD8 T cells.
(A) Representative Phospho-AXL (White) expression and Iba1^{+} leukemia-associated macrophages (Red) by immune-fluorescence in frozen bone sections from vehicle and Bemcentinib treated leukemia bearing mice depicted in B, at final analysis.
(B) Leukemic burden (% GFP^{+} B220^{dim} in bone marrow, spleen and peripheral blood) and spleen pictures of WT mice challenged with 10^3 B-ALL cells and treated twice daily with either vehicle or Bemcentinib at 50 mg/kg. Treatment was initiated on day 4 post leukemia injection and mice were analyzed on day 11. *p<0.05, **p<0.01, two-tailed Student's *t*-test.
(C) Same as B, using CD8 deficient mice. ns, not significant, two-tailed Student's *t*-test.
(**D)** Day 10 leukemic burden (% GFP^{+} B220^{dim} in peripheral blood) in WT mice challenged with 10^3 B-ALL cells treated as in B, in the presence or absence of blocking antibodies against IL12 (300 µg/mouse) and TNFa (400 µg/mouse). Blocking antibodies for IL12 and TNFa were administered daily starting from day 4 post-leukemia challenge. Each dot represents an individual mouse and mean value is depicted. ns, not significant, *, p<0.05, unpaired two-tailed Student's *t*-test.

Author Manuscript Published OnlineFirst on June 8, 2021; DOI: 10.1158/2159-8290.CD-20-1378
Author manuscripts have been peer reviewed and accepted for publication but have not yet been edited.

Figure 7. Systemic AXL inhibition induces potent anti-leukemic immunity and eliminates leukemic blasts in AXL negative leukemias.

(**A and B**) Kaplan-Meier survival curves of C57BL/6 WT mice (**A**) or NSG mice (**B**) challenged with 5.10^5 *Asxl1*$^{-/-}$ AML cells and treated with either vehicle or Bemcentinib (50 mg/kg, twice daily). ns, not significant. ***p<0.001, log-rank (Mantel–Cox) test.

(**C**) Kaplan-Meier survival analysis of C57BL/6 WT mice challenged with 10^3 B-ALL cells and treated with either vehicle (n = 7) or nilotinib (80 mg/kg, once a day) plus Bemcentinib (50 mg/kg, twice daily) (n = 33) for a total of 44 days. Data are pooled from two independent experiments. ***p<0.001, log-rank (Mantel–Cox) test.

(**D**) Representative FACS plots depicting absence of GFP$^+$ B220^{dim} leukemic cells in the bone marrow of long-term survivors from C.

(**E**) Mice from C were followed by weekly bleeding. 3 out of 33 mice (#24, #26 and #31) showed GFP$^+$ cells indicative of disease recurrence and were subjected to anti-PD1 treatment as indicated (7 x 200 µg/ml every 4th day). Mouse#31 succumbed to full blown leukemia on day 36, while #24 and #26 remained leukemia free.

(**F**) Kaplan-Meier survival analysis of NSG mice challenged with 10^3 B-ALL cells and treated with either vehicle, nilotinib or nilotinib plus Bemcentinib for a total of 44 days as in C. ns, not significant, log-rank (Mantel–Cox) test.

(**G**) WT mice were injected with 10^3 TKI^R B-ALL cells. After 5 days, mice were randomly attributed to the indicated vehicle or treatment groups and their survival depicted using a Kaplan-Meier analysis. Data are pooled from two independent experiments**.** ns, not significant, **p<0.01, ****p<0.0001, log-rank (Mantel–Cox) test.

(**H**) Representative FACS plots depicting absence of GFP$^+$ B220^{dim} leukemic cells in the bone marrow of Bemcentinib + vincristine treated long term survivors from G.

In all experiments, treatments were initiated and stopped on the days indicated by dotted lines.

Figure 1

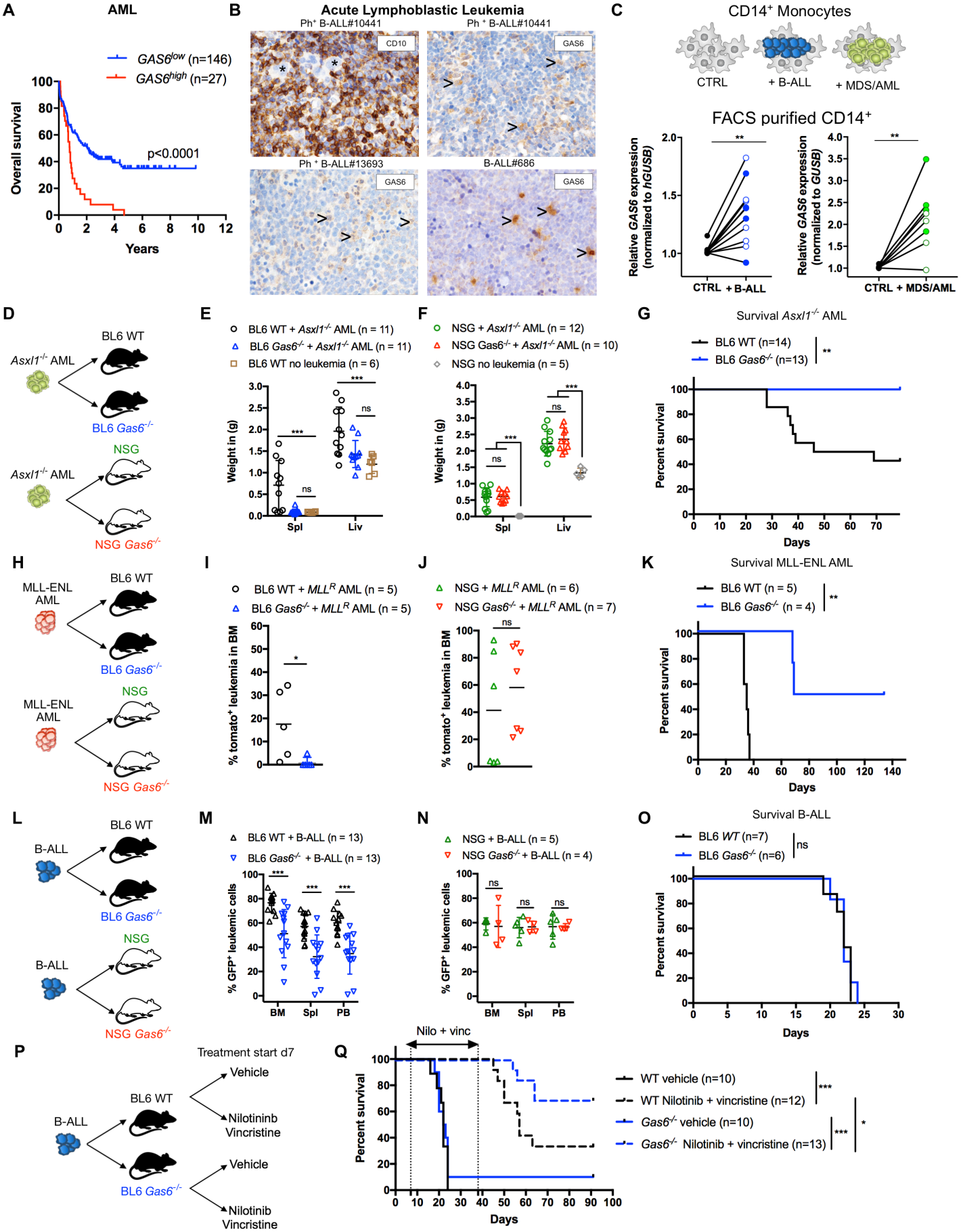

Figure 2

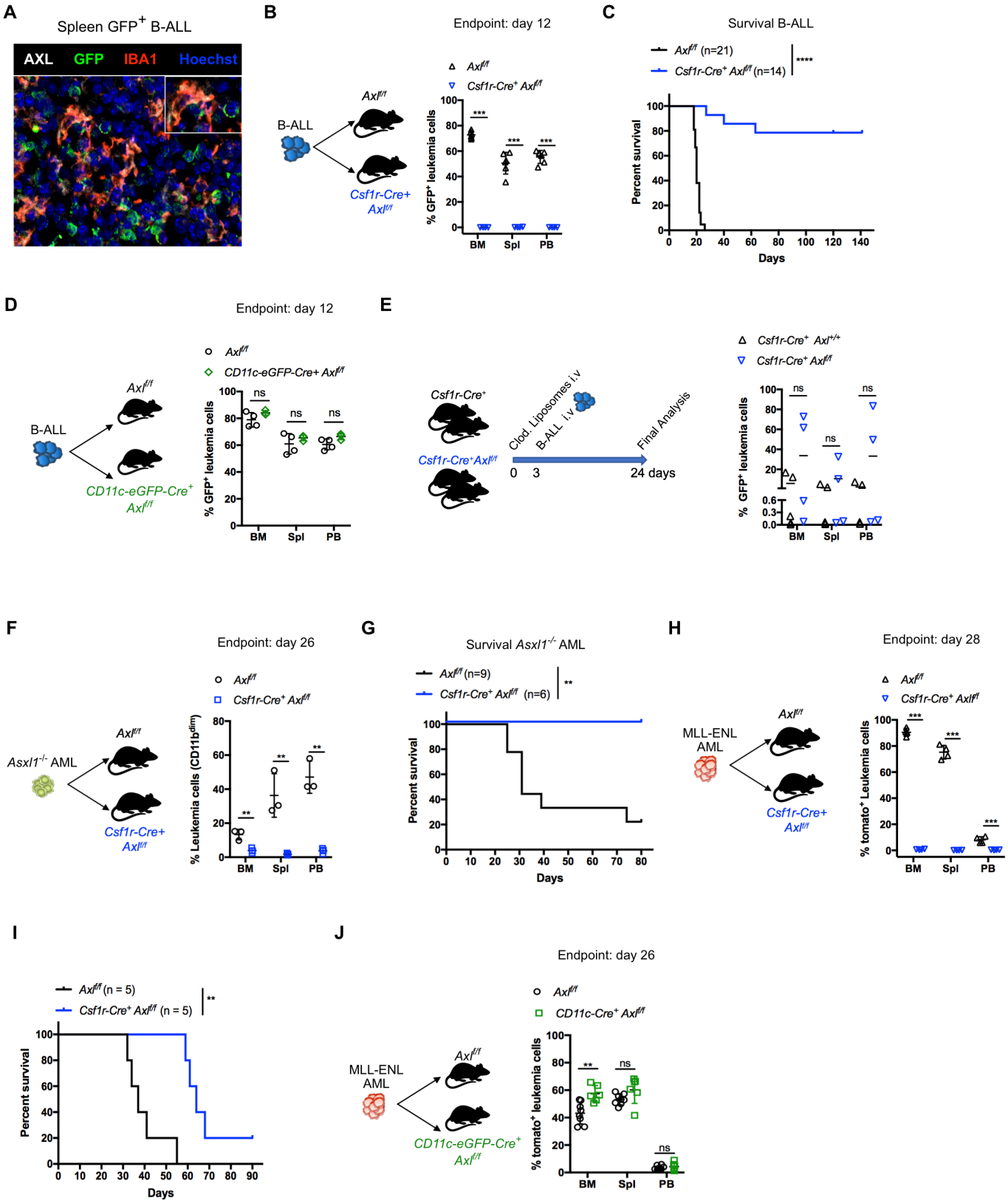

Figure 3

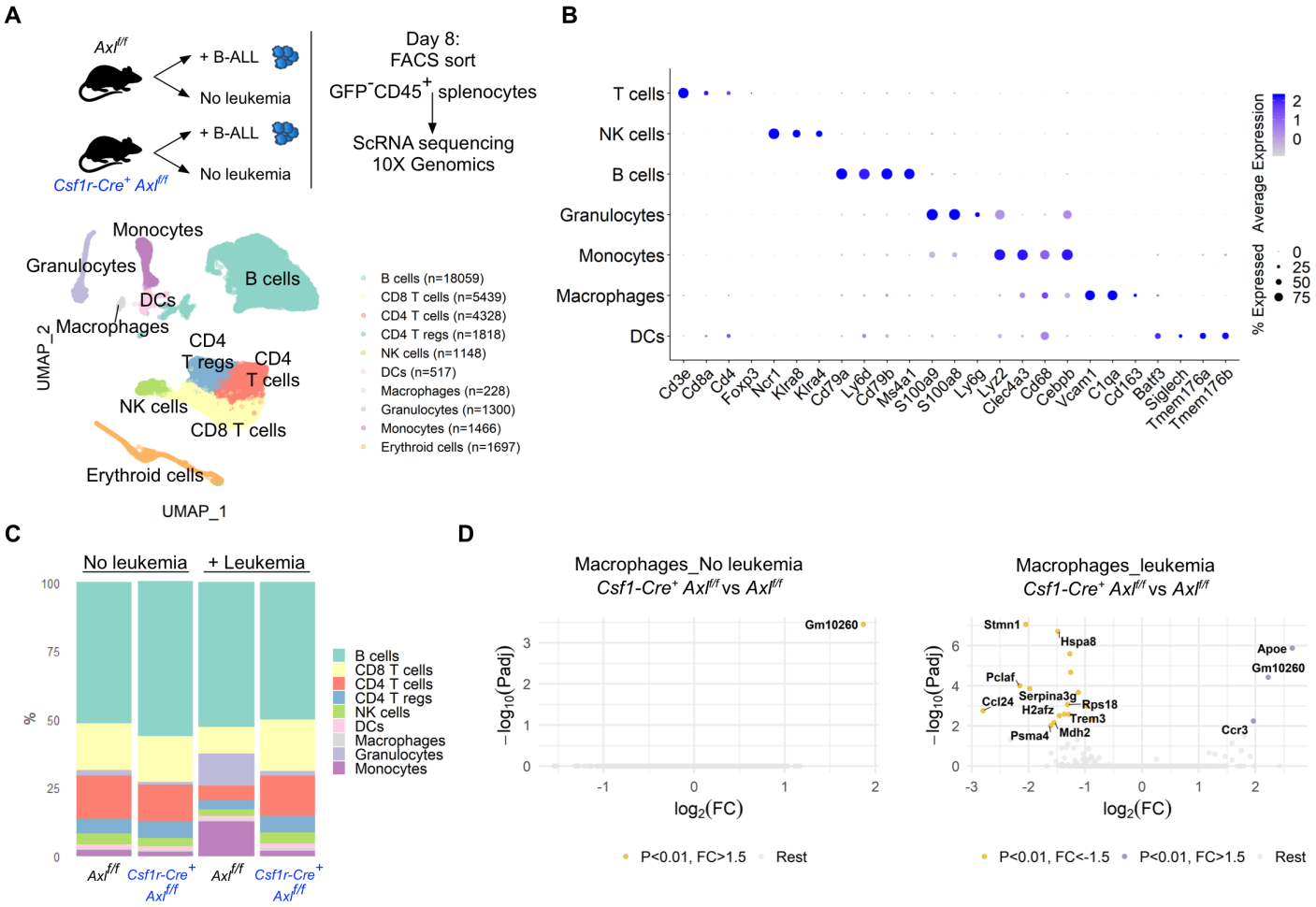

Figure 4

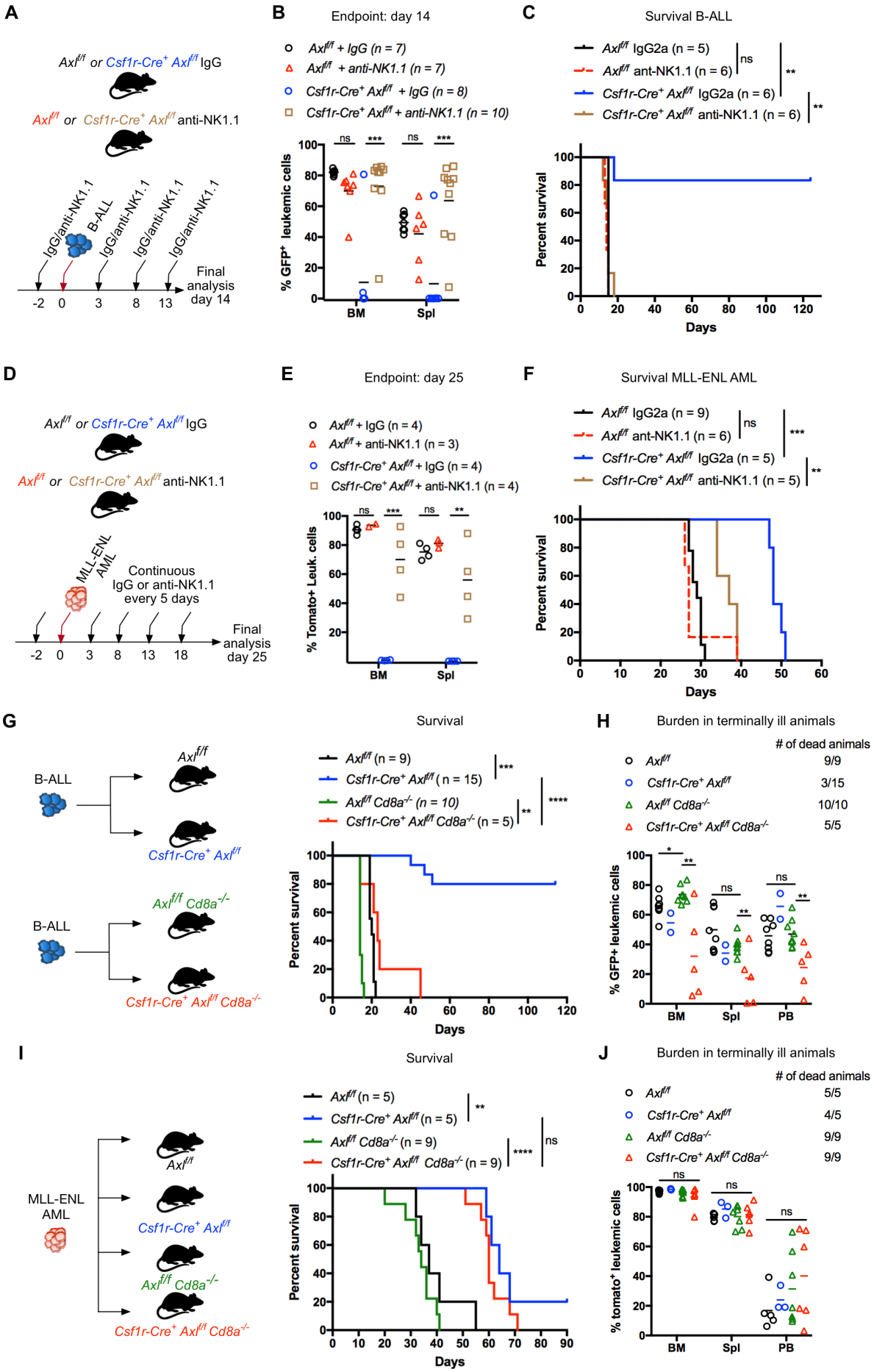

Figure 5

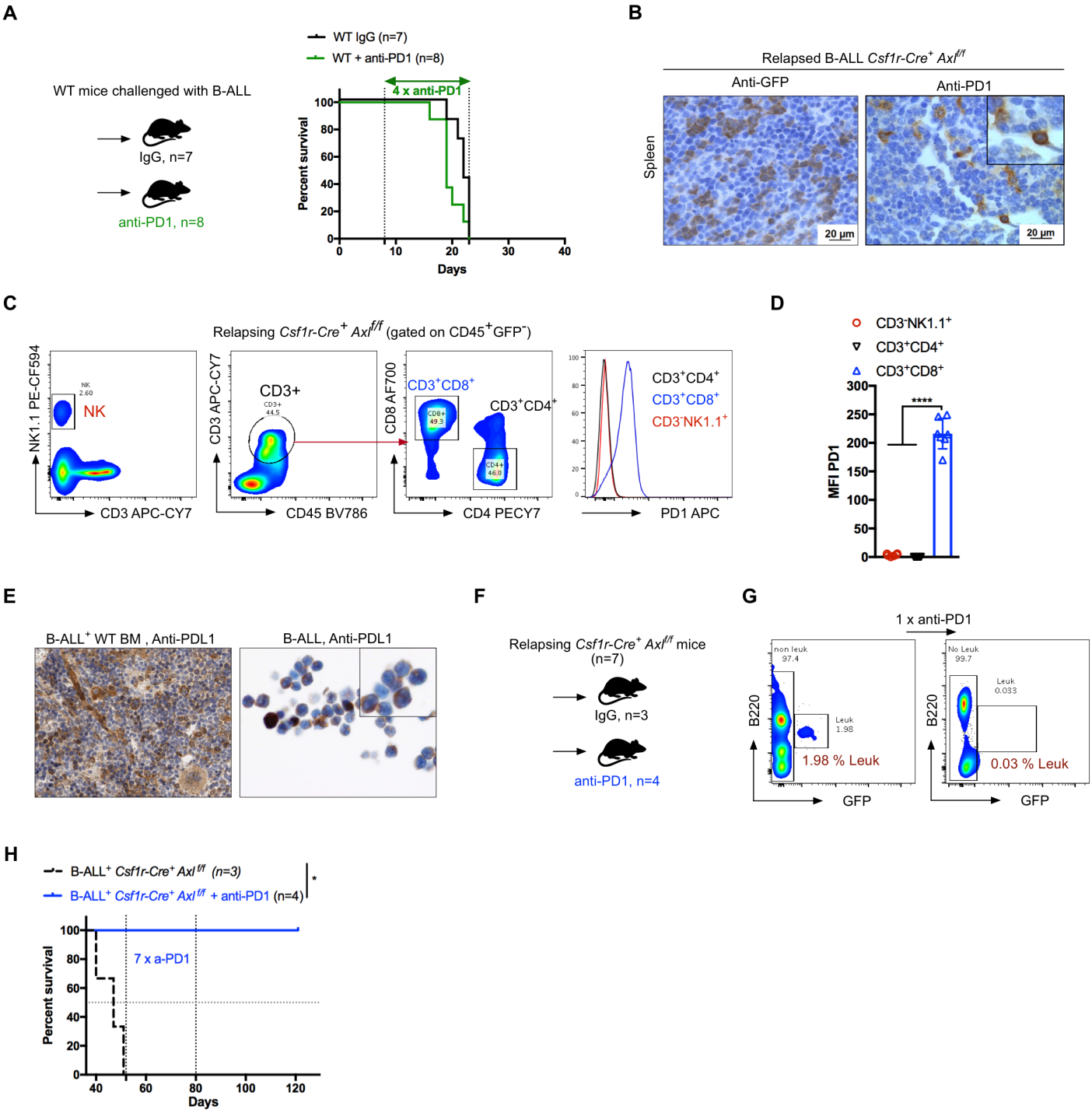

Figure 6

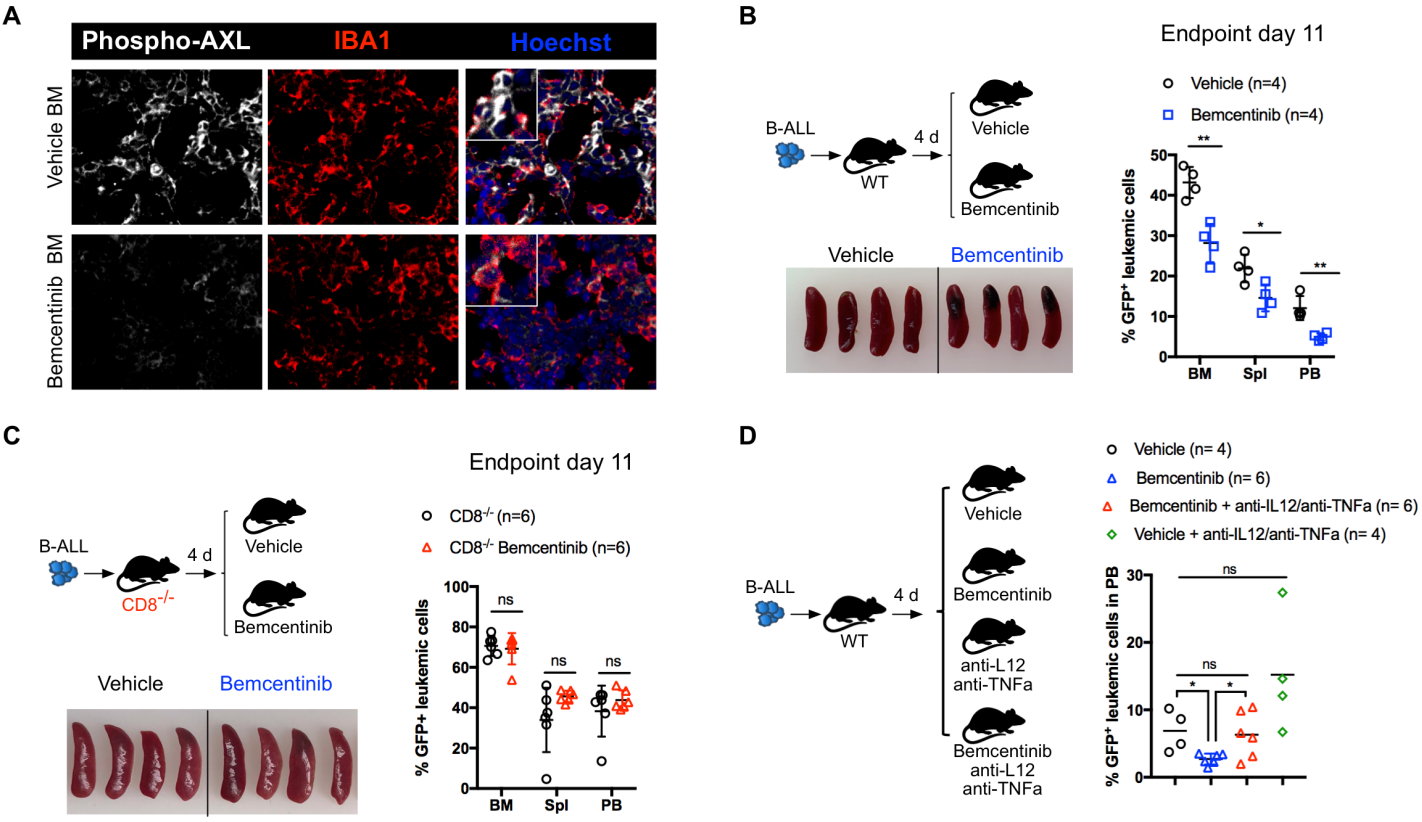

Figure 7

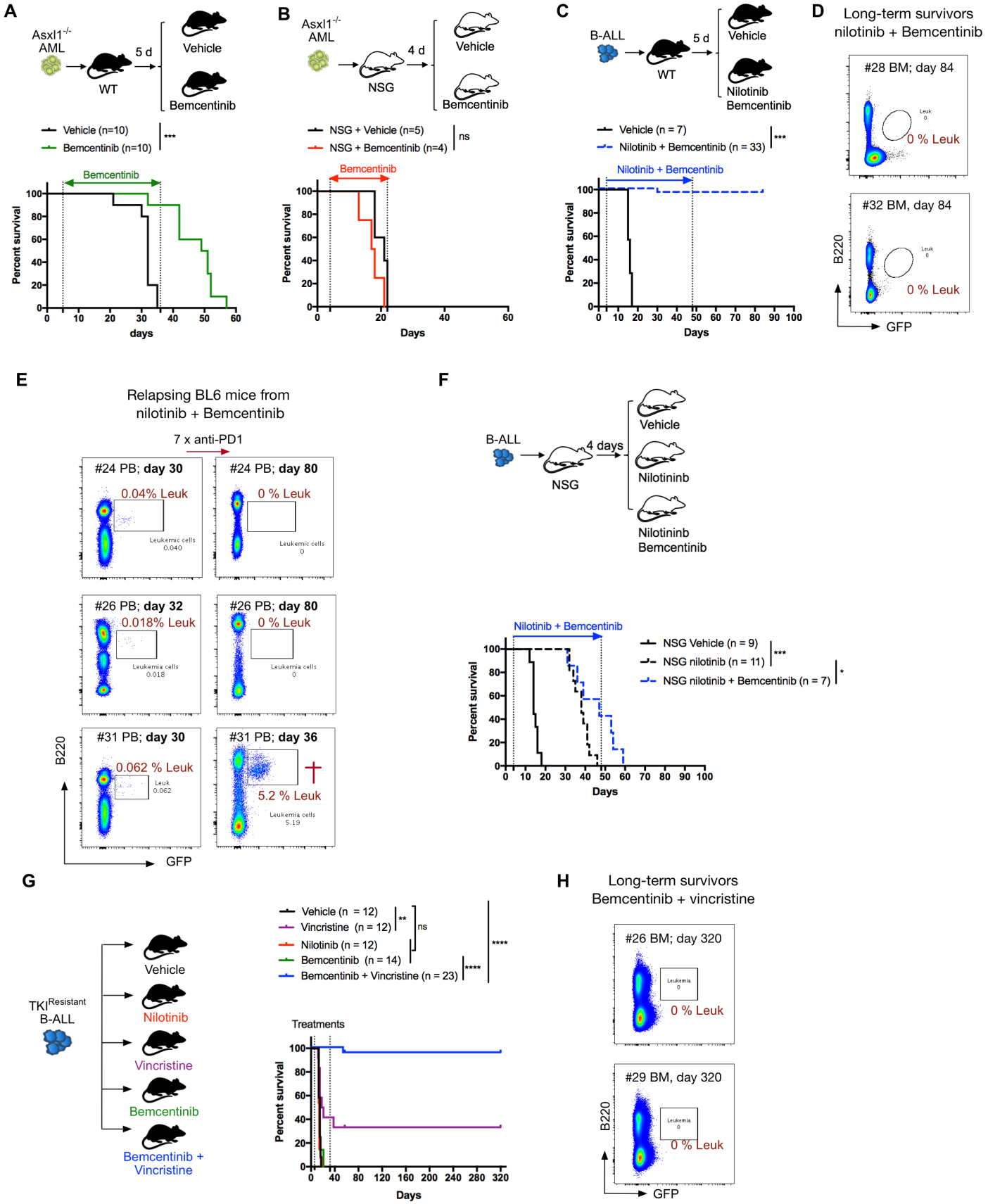

AACR American Association for Cancer Research

CANCER DISCOVERY

AXL inhibition in macrophages stimulates host-versus-leukemia immunity and eradicates naive and treatment resistant leukemia

Irene Tirado-Gonzalez, Arnaud Descot, Devona Soetopo, et al.

Cancer Discov Published OnlineFirst June 8, 2021.